Effects Of
Southern Hemisphere Ionospheric Activity
On
Global Navigation Satellite Systems (GNSS) Based Augmentation System

Low Latitude Threat Model

December 2014

Submitted to:

Servicos de Defesa e Technologia de Processos (SDTP)

And

The U.S. Trade and Development Agency
1000 Wilson Boulevard, Suite 1600, Arlington, VA 22209-3901

Submitted by
Mirus Technology LLC

Prepared by the Mirus Technology, LLC (with Contributions from FAA, Stanford University, INPE, ICEA, Boston College, NAVTEC, and KAIST)

Principal Investigator: Dr. Navin Mathur

Executive Summary

Ground-based Augmentation System (GBAS) augments the Global Positioning System (GPS) by increasing the accuracy to an appropriately equipped user. In addition to enhancing the accuracy of GPS derived accuracy, a GBAS provides the necessary integrity of accuracy (to a level defined by International Civil Aviation Organization, ICAO) required for a system that supports landing of an aircraft at an airport where GBAS is available. In addition, a GBAS system is designed to ensure the process of integrity and required continuity of GBAS operations and associated operational availability.

The integrity of GBAS is threatened by several internal or external factors that can be broadly classified into three categories namely; Space Vehicle (SV) induced errors, environmental induced errors, and internally generated errors. Over the last decade, the US Federal Aviation Administration (FAA) has systematically defined, classified, characterized, and addressed each of the error sources in those categories that apply within CONUS. These efforts culminated in approval of several GBAS Category-I approaches within CONUS at various locations (such as Newark, Houston, etc.).

Through the process of GBAS development for CONUS, the aviation and scientific communities realized that the Ionosphere is one of the key contributors to GBAS integrity threat. For CONUS application, this threat was properly defined, characterized, validated, and mitigated through various monitoring schemes. Additionally, it is a well-known fact that the low-latitude ionosphere is highly erratic when compared to the mid-latitude ionosphere surrounding CONUS. Thus, there is a need to define the low latitude ionospheric behavior so that its impact on GBAS operations in low-latitude regions can be assessed and appropriately mitigated.

This report provides the development and characterization of the ionospheric threat in the Brazilian airspace region of the world. A team of ionosphere research scientists developed a list of 120 days that were deemed stressing for GBAS to meet safety requirements. The selection of days was based upon observed scintillation, kp, and Dst index over the past three years of the current solar cycle (as shown in figure 1 - Sun Spot Number progression as recorded by the U.S. National Oceanic and Atmospheric Administration (NOAA)). Dual-frequency GPS data from various networks within the Brazilian airspace was gathered for those identified days and then analyzed using Long-Term Ionosphere Anomaly Monitor (LTIAM) software developed by the FAA. It is now confirmed that the ionospheric threat to GBAS in the Brazilian airspace is greater than the threat observed in the CONUS region.

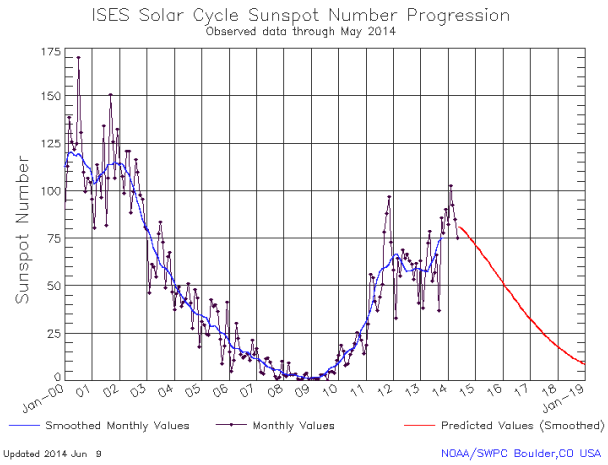

Figure 1. Solar Cycle 24

As stated previously, the team utilized data collected over the last three years, which forms a solid foundation to the development of the threat model. As can be seen from Solar Cycle 24 above, we experienced a much less volatile cycle as compared to Solar Cycle 23. As such the approach taken by the threat model team is generic and flexible enough to be able to update or amend the model trade space as additional data becomes available from subsequent cycles. This approach will ensure flexibility while maintaining operational viability for safety, performance and availability.

The threat model for the low-latitude region (as compared to CONUS) is shown below. As depicted, the data analyst team has identified a several days where the ionospheric gradients threatening to GBAS are in excess of 700-800 mm/km.

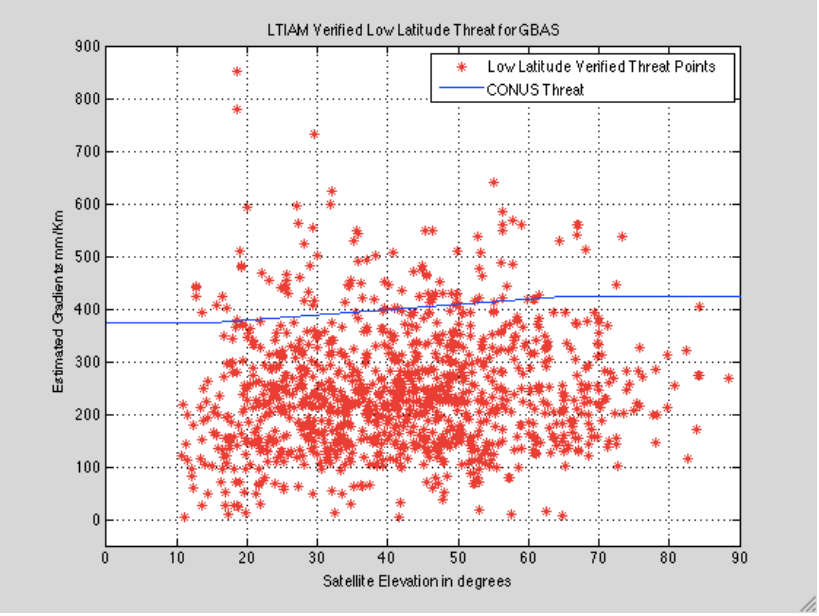

Figure 2. Southern Latitude Threat Model

A few comments about the threat model:

1. The above model represents the ionospheric threat for the entire Brazilian airspace and is not decoupled to highlight the regional variability.
2. All of the threat points depicted in the model above were detected between 2200 and 0500 (UT); the time of high L-band scintillation and ionospheric depletion activity.
3. Many threat gradients that were 200 mm/Km or below were not documented and displayed.
4. For days with multiple high gradients on the same SV and station pairs, only the maximum gradient was documented.
5. Most all gradients were observed on the station pairs that were parallel to the local magnetic force lines.
6. Only a cursory review of the speed of the depletions and their width was performed.

This document contains both a detailed description of the agreed analysis methodology as well as an analysis of the characteristics of anomalous gradients observed in the low-latitude Southern region over the current solar cycles. The results of this assessment indicate that, as far as can be reasonably determined, Southern region (low-latitude) ionospheric conditions, specifically during the post sunset hours, fall outside the bounds of the current ionospheric threat model for Category I GBAS in CONUS. Furthermore, the maximum ionospheric gradient found in this study was 850.7 mm/Km, well above the peak gradient of 412mm/km found during the ionospheric study of CONUS.

Table of Content

Table of Figures

List of Tables

Acronyms

CMC – Code Minus Carrier (ionospheric delay estimation)
CONUS – Conterminous United States
CORS – Continually Operating Reference Station
DECEA – Departamento de Controle do Espaço Aéreo
DoY – Day of Year
GBAS – Ground-Based Augmentation System
GNSS – Global Navigation Satellite System
ICAO – International Civil Aviation Organization
ICEA – Instituto de Controle do Espaço Aéreo
IEAV – Instituto de Estudos Avançados
IGEB – Instituto Brasileiro de Geografia e Estatística
IGS – International GNSS Service
INPI – Instituto Nacional da Propriedade Industrial
IWG – Ionospheric Working Group
IPP – Ionospheric Pierce Point
KAIST – Korea Advanced Institute of Science & Technology
L1 – GPS Frequency (1575.42 MHz)
L2 – GPS Frequency (1227.60 MHz)
LAAS – Local Area Augmentation System
LGF – LAAS Ground Facility
LIP – LAAS Integrity Panel
LISN – Low-Latitude Ionospheric Sensor Network
LTP – LAAS Test Prototype
MASPS – Minimum Aviation System Performance Standards
MIEV – Maximum Ionosphere-Induced Error in Vertical
RBMC – Rede Brasileira de Monitoramento Contínuo do GPS
MOPS – Minimum Operational Performance Requirements
RF – Radio Frequency
RINEX – Receiver INdependent EXchange Format
RNAV – Area Navigation
SARPS – Standards and Recommended Practices
SBAS – Space-Based Augmentation System
SV – Space Vehicles
TDA – Trade and Development Agency
TEC – Total Electron Content
TECU – Total Electron Content Units (1TECU = 10^{16} electrons / m^2)
UT – Universal Time
WAAS – Wide Area Augmentation System
WJHTC – William J Hughes Technical Center

1 Overview and Scope

The project was conducted as an international, interagency effort with Mirus Technology as the Prime US contractor and project lead with support from scientists and engineers at the FAA Technical Center, Stanford University, Boston College, INPE, ICEA, IEAV, UNESP, FAATC/NAVTAC, KAIST, and the Catholic University in Rio de Janeiro. This highly critical capability is essential to enable continued transition of GNSS technologies (such as GBAS) to global aviation. The above team provided some of the world experts in ionosphere, GNSS, GBAS, and safety certification to ensure that the generated threat model for GBAS is operationally suitable for use in the international aviation arena.

Figure 3 below depicts the data analysis interaction flow between various groups and organizations (that supported this effort) to ensure that consensus was achieved throughout the analysis process. The core technical advisors were Mr. John Warburton from the FAA technical Center, Dr. Sam Pullen from Stanford University, and Dr. Patricia Doherty from Boston College. The core analyst team included members from FAA, NAVTAC, KAIST, INPE, Boston College, and MIRUS.

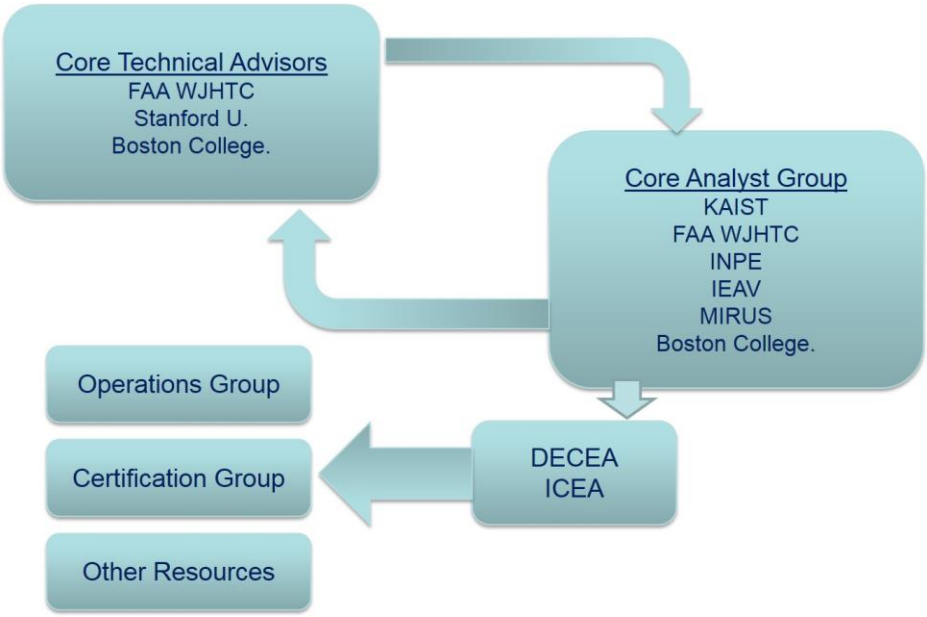

Figure 3. Threat Model Data Analysis Flow

The US GBAS threat model was assembled based on observed ionospheric storm data collected within the continental United States (CONUS). The US threat model development effort was focused on only CONUS ionospheric threats in order to certify the first Category I (CAT-I) GBAS installations at Newark and Houston. The FAA team leveraged data available from the FAA Wide Area Augmentation System (WAAS) and Continually Operating Reference Station (CORS)

measurements to provide a dense network of measurements for ionospheric anomaly characterization. Unfortunately this data is not applicable to low-latitude characterization due to the unique aspects of ionospheric storms in the southern latitudes however the methodologies, analysis, and organizational structure were followed in order to maintain consistency and continuity. Therefore, in order to develop a viable threat model for the southern latitudes a similar effort is required in Brazil.

GBAS will be a key capability required to provide the technical foundation to modernize various Global Navigation Satellite System (GNSS) capabilities that will serve as the cornerstone of the modernized Brazilian aviation infrastructure and support a large number of other commercial and governmental objectives that require precise positioning. To that end, Servicos de Defensa e Tecnologias de Processos (SDTP), a federally mandated foundation, with concurrence of DECEA, has supported and overseen the execution of the development of this Ionospheric Threat Model effort.

The project progress was monitored through regular communications using regular meetings and teleconferences. In addition, a secure FTP site was utilized so that data and documents could be posted for authorized team members to maintain working documents, data analysis, and identified issues for resolution. The team collected historical, empirical, and new ionospheric data to create a complete data set covering all of the Brazilian landmass. Data was collected from various existing GPS monitoring networks including RBMC/IBGE, LISN, CIGALA, SIPEG, Honeywell, and FAATC LAAS Test Prototype (LTP). Additionally, DECEA and the FAA have been collecting ionospheric activity data in Southern Hemisphere for many years. This data was identified, collated, catalogued, and analyzed for specific events that could possibly impact GBAS operations.

The threat model was developed using the following approach:

- Use CONUS effort as a baseline and the tools and procedures developed by the FAA for the CONUS ionospheric threat model. Leverage assumptions made by the FAA as necessary.
- Identify necessary and relevant data to be collected using network of GPS data sources for all of Brazil.
- Identify days-of-interest based on space-weather indices (Kp and Dst) and L-band Scintillation parameter (S4).
- Process data for the identified days-of-interest and document the threat model.
- Determine and characterize the lower latitude ionosphere.
- Validate and deliver operational threat model.

This document contains the culmination of efforts to characterize the ionospheric threat posed to a GBAS facility in the low-latitude region of the world; specifically over the Brazilian airspace.

2 Background

2.1 Ionosphere

The ionosphere is a layer of the upper atmosphere located roughly between 50 km and 1000 to 1200 km above the Earth's surface, which gets ionized by solar extreme ultraviolet (EUV) and other emissions from the sun. The structure of the ionosphere is not constant but is continually varying in response to changes in the intensities of solar radiations. Thus, delays in the propagation of GNSS signals from satellite to receiver due to the ionosphere vary with time as well as with the locations of the receiver and the satellite.

Figure 4 shows the daily-recorded sunspot variability from 1900 until 2013.

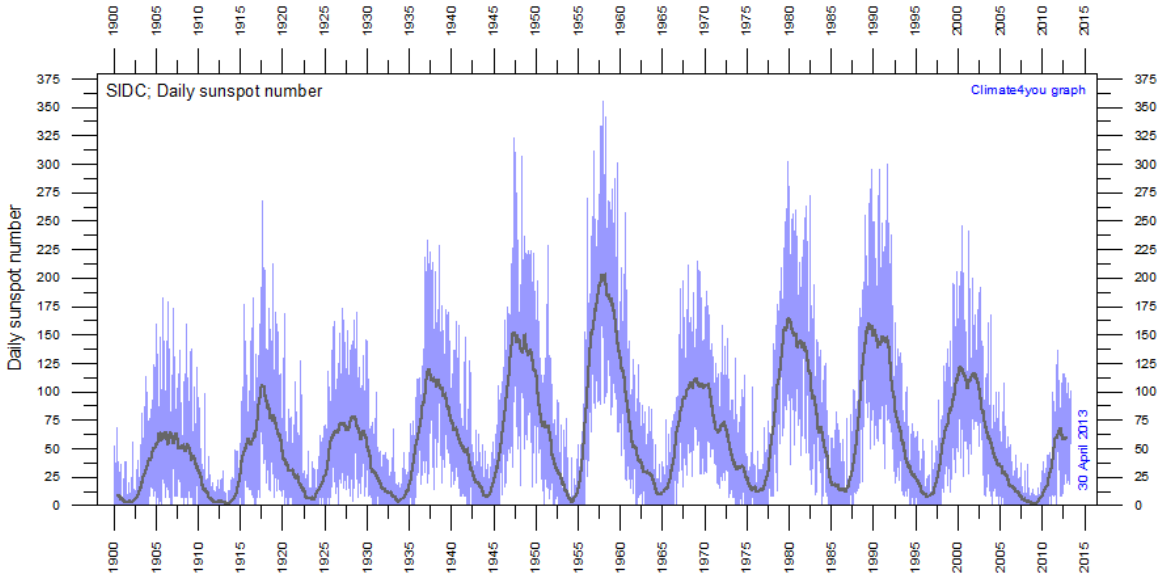

Figure 4. Daily Sunspot variability from 1900 to present

There is a direct correlation between the recorded sunspot numbers to the intensity of the solar radiation experienced by the Earth's upper atmosphere. An increase in solar activity (more sunspots) is accompanied by an increase in the "solar wind," which is an outflow of ionized particles, mostly protons and electrons, from the sun. Far more variable than changes in total solar irradiance are changes in amount of energy emitted as ultraviolet, extreme ultraviolet, and X-rays, and in the continuous outflow of ionized solar particles (solar wind), which controls the properties of the Earth's atmosphere. The connection between solar activity, as measured by what solar physicists refer to as "coronal mass ejections" or CME's, and geomagnetic storms has been well documented in recent years.

There are three regions of the world as classified based on ionospheric activities. They are: 1) the mid-latitudes, 2) the auroral and polar caps, 3) the equatorial and equatorial "anomaly"

regions. Figure 5 illustrates the approximate geographic extent of each of these regions with the mid-latitudes hemmed between the transitional region and the equatorial region in this plot. By far the largest region is the equatorial anomaly region, the effects of which can be measured up to ±30°-40° geomagnetic latitude, which is 50% of the earth's surface and covers much of the Brazilian Airspace. Most part of the CONUS is located in the mid-latitude region of the world. Under nominal conditions, the ionospheric activity over the mid-latitude regions is undisturbed with predictable ionospheric behavior. Severe ionospheric storms are rare in mid-latitude regions but can cause severe degradation to GBAS service. The CONUS threat model is based on occurrence of one such storm over US that caused significant anomalies that could potentially threaten GBAS safety of operations.

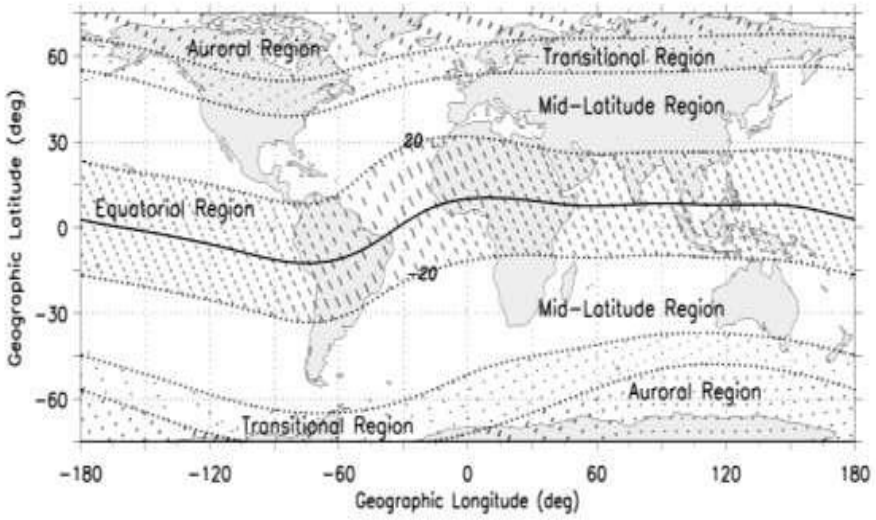

Figure 5. Ionosphere regions of the world (From SBAS Iono WG)

The equatorial regions have larger range delay gradients, a large occurrence of scintillation effects, and, in some cases, larger day-to-day variability in range delay than the mid-latitude ionosphere. The behavior of the ionosphere, as far as its observable effects on radio signals is concerned, varies with time and location.

Ionospheric Behavior in Equatorial Regions: The equatorial anomaly regions, those regions of the earth's ionosphere located at approximately ±20° on either side of the magnetic equator have the highest values of Total Electron Content, (TEC), directly proportional to ionospheric range delay, in the world. These regions of very high TEC are produced, not directly by the solar EUV, but by an E x B force that causes what has been termed the "fountain effect" in the earth's ionosphere. The equatorial fountain varies from day to day, and can vary considerably over different longitudes, making the absolute variability of TEC largest in the anomaly peak regions.

GPS satellites are about 22,000 Km above the surface of the Earth and hence the signal transmitted by the GPS satellite travels through the ionosphere and acquires a flavor of ionosphere at that instant; for a particular line of sight between the satellite and the receiver on the surface of the Earth. Since GPS signals are available on two different frequencies (L1 and L2), this dispersive impact of the ionosphere shows up on both signals; but differently. This difference of ionospheric impact on the two frequencies is deterministic; thus, using GPS measurements on both frequencies, and using validated models, the ionosphere part of the impact can be separated, to some extent. Figure 6 (Courtesy Boston College) below shows one example of the ionospheric storm measured using the dual frequency receivers within LISN network.

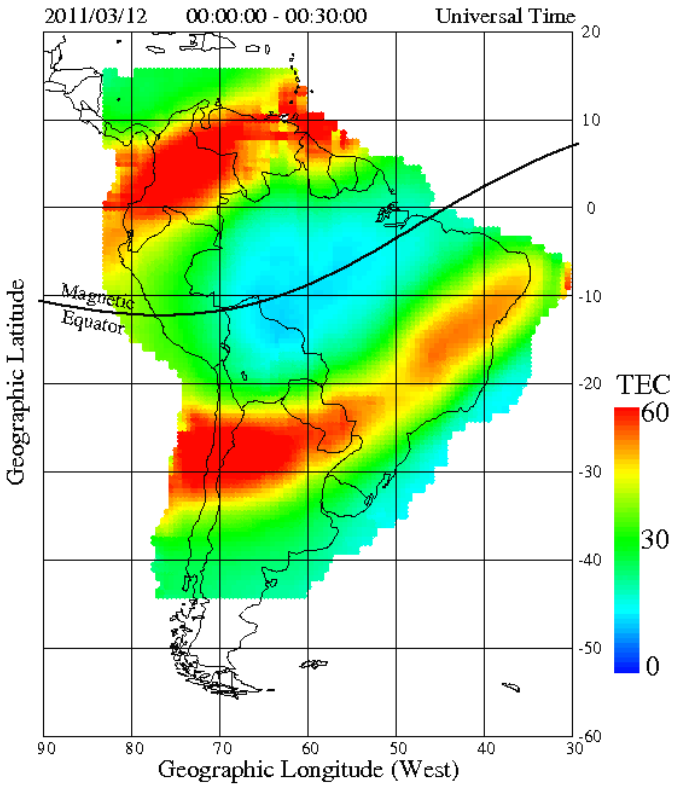

Figure 6. LISN network storm measurements

The second potentially major issue with ionospheric range delay in the equatorial region is that of large depletions in ionospheric range delay, associated with the onset of plumes of irregularities that produce strong amplitude scintillation fading and phase scintillation effects in the post-sunset local time period. During higher solar activity peaks, during certain seasons, post sunset, the upper ionosphere becomes unstable due to disturbances produced by gravity waves or some other source. This instability (often referred to as Rayleigh-Taylor instability) can generate ionospheric irregularities through depletions within the ionosphere. These depletions are also referred to as ionospheric bubbles, and these bubbles can be of various sizes (from several meters to 10s of Km) and speed (from ~70 m/s to up to 250 m/s) [11]. These bubbles also have tendency to move from

west to east under the influence of Earth's magnetic field. They are most frequent during the equinox seasons, slightly less frequent during the winter, and relatively rare during the summer.

One example of the large variation of slant delay measured by two stations within the Brazilian airspace is shown in figure 7 below. This figure shows the measured slant ionospheric delay on SV01 as measured from two stations, SJSP and SJCU, located 9.72 Km away from each other. The slant delay clearly shows feature of Equatorial Plasma Bubbles (EPB) on the GPS estimate of ionospheric delays.

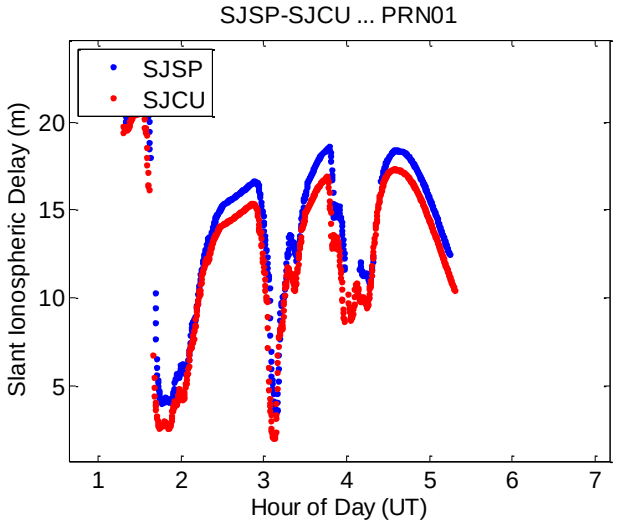

Figure 7. Slant delay measurement

Gentile et al. [14] developed a global climatology of EPB using measurements made from the Defense Meteorological Satellite Program (DMSP). Figure 8 below shows the rates of plasma bubbles as measured by DMS from 1999 to 2000. It indicates higher plasma bubble rates from September until April of those years of enhanced solar activity (peak of Solar Cycle #23) – specifically over the geographical area of equatorial latitudes over Southern American continent.

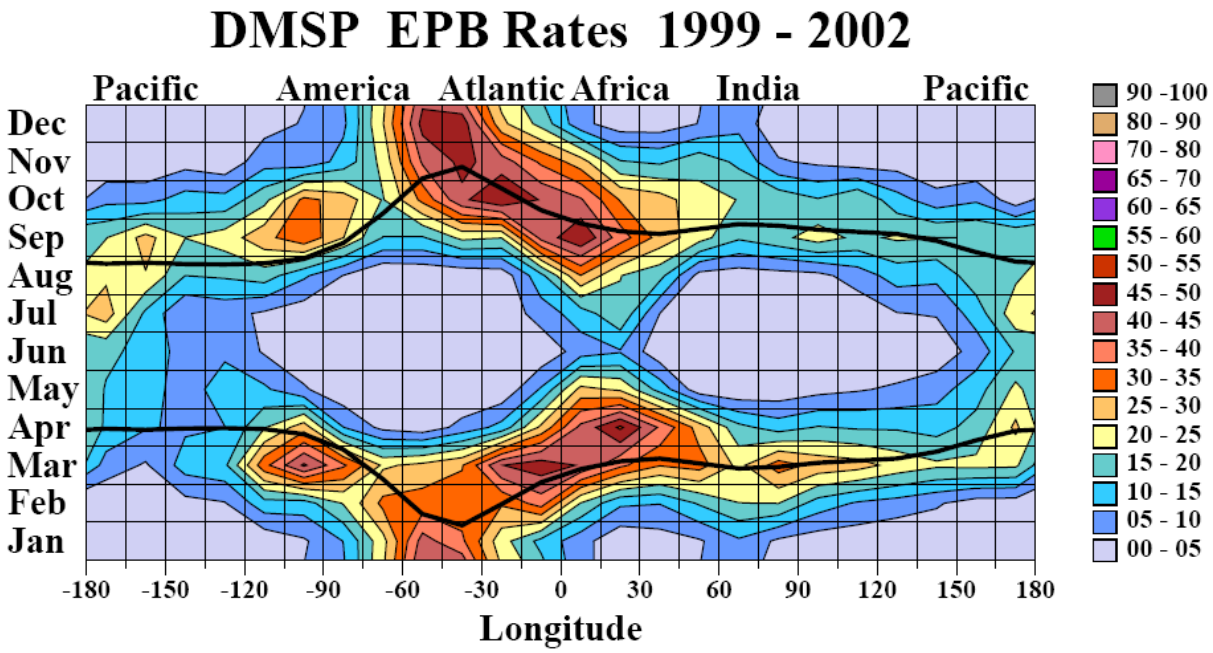

Figure 8. Rates of plasma bubbles [14]

The same study also observed a lack of EPB during the waning part of the solar cycles. Hence, the presence of post sunset EPB are not only location and time-of-day dependent, they are also dependent on the season within a year and the phase of the solar activity cycle. Finally, these phenomenon's can also vary as a result of rare geomagnetic (ionospheric) storms caused by powerful energetic emissions from the sun.

2.2 Ground Based Augmentation System

GBAS is a civil-GPS ground-based augmentation system that augments GPS based measurements to provide the required accuracy and safety for precision approach to an aircraft equipped with GBAS airborne equipment, for the supported airport. Additionally, GBAS provides RNAV capability within the terminal area. The safety of operation is assured by the GBAS by ensuring that the system meets the allocated integrity and continuity for the supported operations.

GBAS consists of a ground facility that provides the measurement corrections and associated integrity parameters to the airborne user using a VHF data link. The ground facility also provides the approach path information to the airborne users. The airborne user/receiver utilizes the transmitted corrections to assess/compute the necessary parameters to assess the system performance. Figure 9 shows the top-level architectural components of GBAS.

It is the responsibility of the GBAS and GBAS service provider to ensure that the transmitted integrity parameters address all possible safety threats to GBAS to the level of integrity for the

supported level of operation. The threat to GBAS includes potential errors or failures in the GPS space segment, ground segment or environment (to include the space environment and ground facility environment). Ground Based Augmentation Systems (GBAS) can correct the majority of the GNSS pseudo range errors experienced by an aircraft in the vicinity of an airport. Not corrected (spatially uncorrelated) errors between the ground and airborne subsystems must be overbounded and kept as small as possible in order to reach the required level of integrity defined by ICAO.

The GBAS requirements are defined in the ICAO SARPS and for the case of the US Federal Aviation Administration (FAA) are further elaborated in the RTCA LAAS MOPS (DO-253A), Local Area Augmentation (LAAS) MASPS (DO-245A), and the FAA Non-Fed Category-I LAAS Ground Facility Specification (FAA-E-3017).

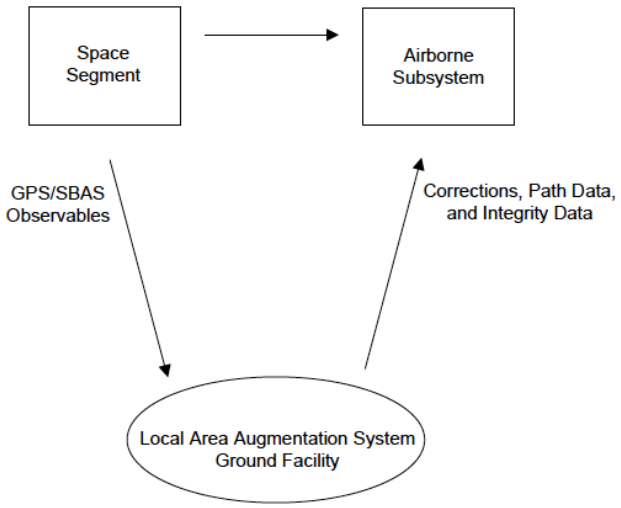

Figure 9. GBAS Architecture (FAA-E-3017)

The ICAO SARPS (Annex 10 – Volume I) provides the internationally harmonized standards and recommended practices for all the navigational aids. It contains high-level requirements for GBAS as well. LAAS MASPS defines the overall architecture and requirements of the US GBAS system (called Local Area Augmentation System). The RTCA MOPS contains the minimum operational requirements for the LAAS airborne equipment. The RTCA LAAS ICD is the interface control document between the ground facility and the airborne equipment. Finally, the Cat-I LGF specification contains the non-federal LAAS Category-I ground facility requirements. Thus the entire capability of GBAS is articulated within the requirements contained within ICAO SARPS (internationally harmonized requirements), MOPS (Airborne requirements), ICD (interface between ground and the airborne system), and the ground Specification.

2.2.1 GBAS Requirements

Table 1 below includes the Signal in Space parameters for Category–I GBAS as defined in ICAO SARPS.

Table 1. GBAS Signal in Space requirements

Accuracy Horizontal 95%	16.0 m (52 ft)
Accuracy Vertical 95%	6.0 m to 4.0 m (20 ft to 13 ft)
Integrity	$1 – 2 \times 10^{-7}$ in any approach
Time to Alert	6 seconds
Continuity	$1 – 8 \times 10^{-6}$ per 15 seconds
Availability	0.99 – 0.99999
Vertical Alert Limit	35.0 m to 10.0 m (115 ft to 33 ft)
Horizontal Alert Limit	40 m (130 ft)

Definitions for each of these terms along with their relevance to GBAS approach is defined in ICAO SARPS – Annex 10 as well.

2.2.2 GBAS Ground Station Integrity

The integrity for GBAS (noted in Table 1), as allocated to the GBAS ground station is defined as (FAA-E-3017): The probability that the LAAS Ground Facility transmits out-of-tolerance precision approach information for 3 seconds or longer due to a ranging source failure, LGF failure, anomalous environmental or atmospheric effects, when operating within the Radio Frequency Interference (RFI) environment defined in appendix D of RTCA/DO-253A, shall not exceed 1.5×10^{-7} during any 150-second approach interval.

As can be gleaned from the definition above, the integrity of the GBAS is challenged from several threats. A list of threats to a GBAS is listed below.

Ranging source failures:

- Signal Deformation
- Low signal power
- Code Carrier Divergence
- Excessive Pseudorange acceleration
- Erroneous broadcast of GPS ephemeris data

Environment induced errors:

- Radio Frequency Interference (RFI)
- Environment around ground station (multipath etc)
- Ionosphere and Troposphere variability

Hardware/Algorithms/Operator Induced Errors:

- VDB transmission errors
- Consistency of performance across various GPS receivers
- GBAS corrections fail the overall sanity checks
- Hardware failure etc.

The LAAS ground facility is designed to mitigate the impact of these errors sources such that the allocated integrity and continuity of the system is maintained. Ionospheric variability and its impact on the GBAS performance has been one of the most challenging aspect of GBAS design. Due to the unpredictability of the ionosphere, the modeling the ionospheric threat to GBAS and the associated validation of the model required large amount of relevant data. This effort put the boundaries on the ionospheric threat model and subsequently the threat mitigation procedure was established and implemented.

2.3 Ionospheric threat to GBAS in CONUS

The GBAS ground facility is solely responsible for protecting a user from all integrity threats within the GBAS service volume. Thus, the GBAS ground facility has the responsibility to detect the ionospheric conditions that can cause the failure in meeting the allocated integrity of the ground facility. This capability is achieved by using $\sigma_{vert\_iono\_gradient}$, an integrity parameter transmitted from the ground station to the airborne GBAS equipment. $\sigma_{vert\_iono\_gradient}$ is one sigma value for nominal ionosphere vertical spatial gradient and is transmitted in Message Type 2. The airborne equipment utilizes the value of $\sigma_{vert\_iono\_gradient}$ to estimate the residual ionospheric uncertainty for a given satellite using the following expression.

$$\sigma_{iono} = F_{pp} \times \sigma_{vert\_iono\_gradient} \times (x_{air} + 2 \times \tau \times v_{air}) \text{ where}$$

F_{pp} = the vertical-to-slant obliquity factor for a given satellite;
x_{air} = the distance (slant range) in meters between current aircraft location and the GBAS reference point indicated in the Type 2 message;
τ = 100 seconds (time constant), and
v_{air} = the aircraft horizontal approach velocity (meters per second).

σ_{iono} is then used to compute the Vertical Protection Level (VPL)'s in the airborne equipment. VPL value overbounds the GBAS errors to ensure the integrity of the system.

For CONUS, under nominal conditions, ionosphere gradients remain small (can be bounded by 4mm/km in the mid-latitude regions). This "normal" behavior of the ionosphere has a very limited impact on the position error and the associated VPLs. In this case, the GBAS provided user position is fully acceptable for precision approach.

For CONUS implementation, the non-nominal ionospheric condition for GBAS is referred to as the Storm condition. The ionospheric activity caused due to interaction of solar induced radiations on Earth's atmosphere, which in turn causes irregularities in the TEC in the ionosphere, is referred to as Ionospheric Strom. These irregularities in the atmosphere can cause events of high or low TEC densities around the world. These irregularities can extend for hundreds of Km and can last from minutes to hours. In reference to GBAS, these events that are caused by ionospheric storm conditions can cause severe integrity threat. When GNSS signals received by the aircraft are delayed in a different way than the GNSS signals received by the GBAS ground facility (GGF), the corrections provided by the GGF can cause unacceptably large position errors at aircraft level. Uncorrected ionospheric delays can cause position errors of several tens of meters even during quiet ionospheric conditions.

Figure 10 shows one of the most extreme GBAS threat scenarios where the ionospheric storm front event develops and follows the GBAS user in the same direction and at the comparable speed. In this scenario, the errors build up for the GBAS user since the GBAS corrections do not account for this gradient (since the ionospheric threat is not visible to the GBAS ground station). The GBAS ground station must address this extreme condition even though the effect is not observable to it.

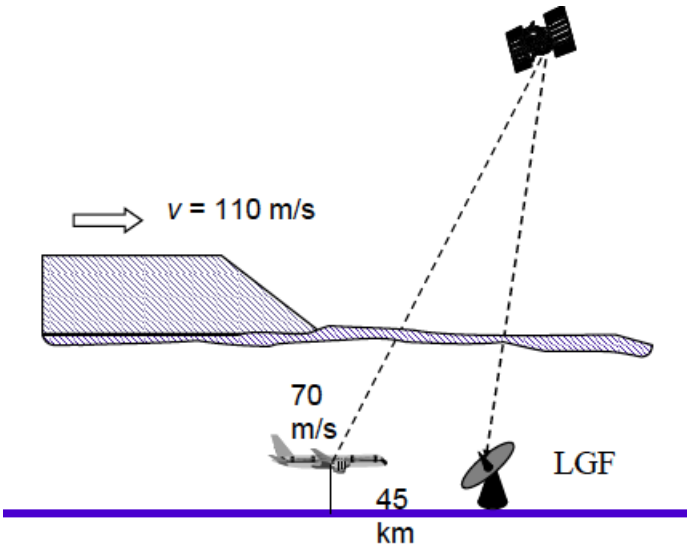

Figure 10. Ionospheric Threat to GBAS user [12]

Figure 11 shows the model developed by the FAA (and Stanford University) of the ionospheric storm as a wedge shaped front with a specific speed, width, and gradient.

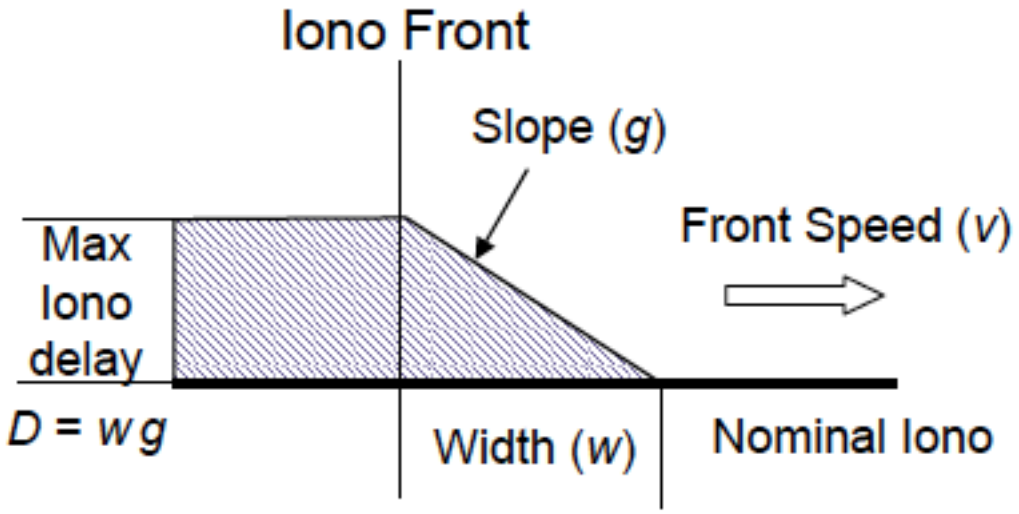

Figure 11. Ionospheric Wedge Model [12]

The FAA scientists and engineers used historical data gathered from WAAS and the CORS ground stations (with currently more than 1800 dual frequency reference GPS receivers) over last decade and more, and used it to characterize the parameters of the ionospheric storm model as depicted above. Figure 12 below shows the most extreme ionospheric variability observed over the CONUS region (near Ohio Michigan area) on November 20, 2003.

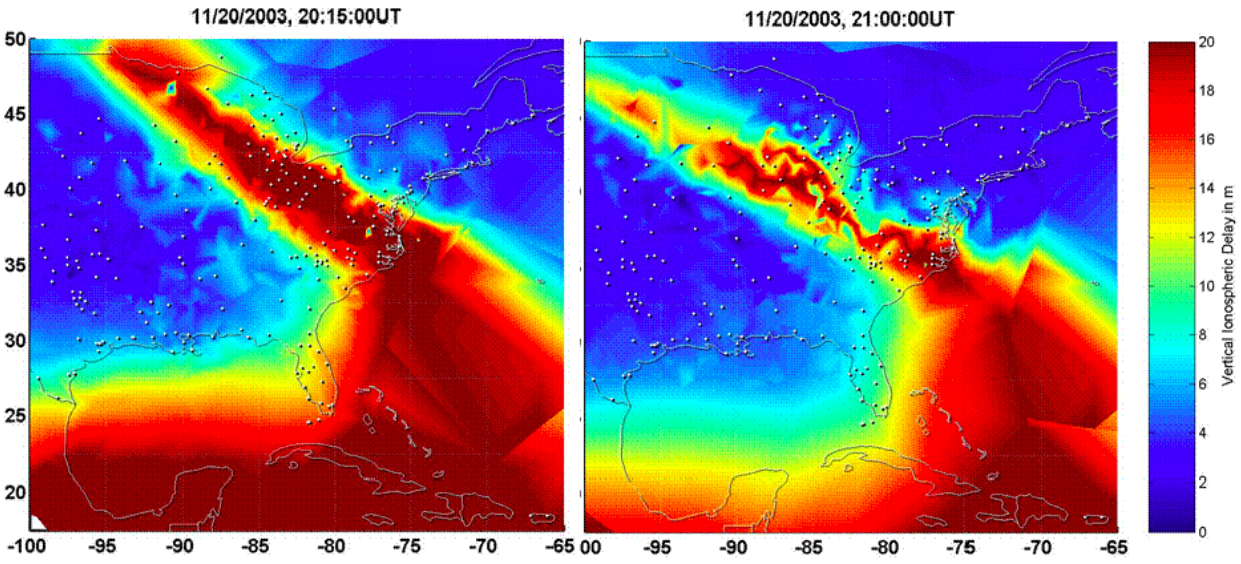

Figure 12. Ionospheric Storm over Ohio (during November 20, 2003) [15]

A detailed analysis of data measured using the CORS network for this day revealed a maximum gradient of 413 mm/Km. The results of such data analysis eventually took shape as the CONUS threat model shown in the Figure 13 below.

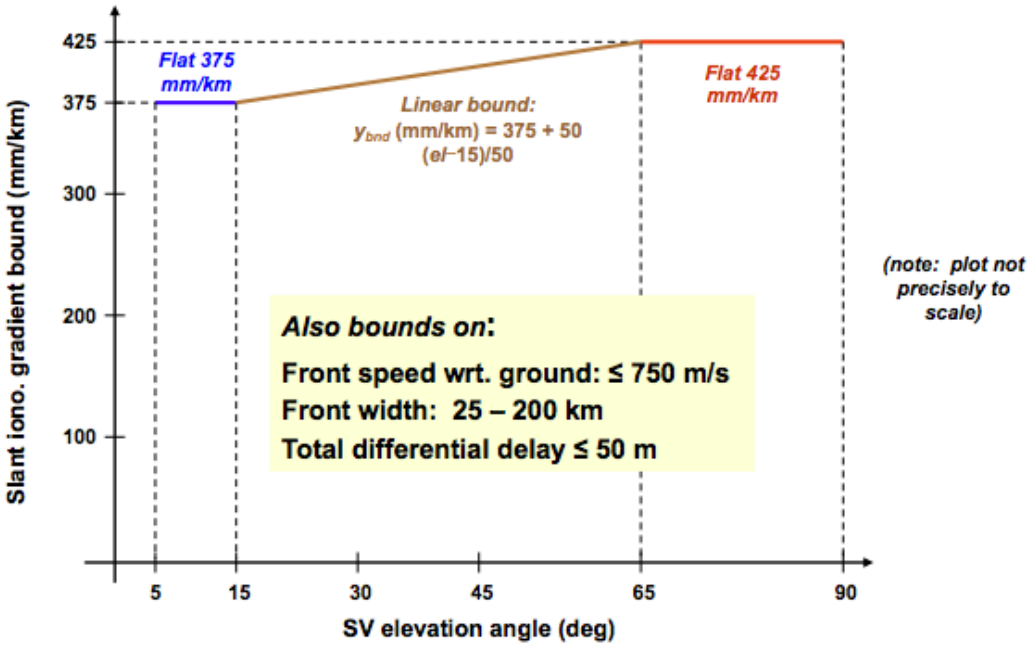

Figure 13. CONUS Ionospheric Threat Model for GBAS [12]

Additionally, based on the observed data, bounds were established on the speed of the front with respect to the ground (up to 750 m/s), width of the front (between 25 and 200 km), and total differential delay (up to 50 meters). These boundary conditions are then used to demonstrate the safety of LAAS in CONUS.

3 Low-Latitude GBAS Threat Model

The approach and procedure followed to generate the low-latitude ionospheric threat model for GBAS leverages the developments made during the CONUS threat model generation. Data collected by various dual-frequency receivers from the CORS network and the WAAS reference stations were processed to identify the largest gradient observed for any given station pair and for any SV. All of the estimated gradients (with some added margin) were used to form the threat model that was mandated to be applicable over the entire CONUS.

The process of generating the low-latitude threat model is as follows:

1. Establish data processing philosophy (Section 3.1)
2. Select days to process the GPS data (Section 3.2)
3. Gather all available GPS data (Section 3.3)
4. Process the data using LTIAM (Section 3.4)
5. Generate the threat model (Section 3.5)

3.1 Data Processing Philosophy

The ionosphere disperses the two frequencies of GPS (L1 and L2) differently but predictably. Dual-frequency GPS measurements from a network of dual-frequency receivers that are located at precisely surveyed locations can be used to estimate the ionospheric delays. However, in addition to the ionosphere, the GPS signal traversing through space to the user's antenna, acquires several other features. Some of these features that are added to the GPS signal are – amplitude and phase noise due to scintillation, multi-paths due to reflective surfaces in the vicinity of the user, tropospheric variation, and signal noises due to radio frequency interference near the antenna. In addition to these, there are errors introduced within the measurements due to satellite clock errors and user hardware related errors (such as inter-frequency biases).

Ionospheric variations and these other noises/errors sources are then processed through the GPS receiver tracking loops and eventually manifest themselves as errors on the measurement of Pseudoranges and Carrier Phases for each satellite. During this process, the GPS receiver adds noise, measurement errors due to the movement of the signal on two frequencies within the antenna and the receiver tracking loops. Psuedoranges and carrier phase measurements on L1 and L2 frequencies are the relevant measurements from the receiver that can be used for studying the behavior of all the above mentioned noise/error sources. Decoupling these error sources from each other using the GPS measurements on both frequencies involves careful data analysis, error estimation, and study of conditions where the error sources may be observable. This process requires understanding of the error sources, their behavior and characteristics along with their impact on the signal measurements.

Figure 14 below shows an animation of the problem statement above.

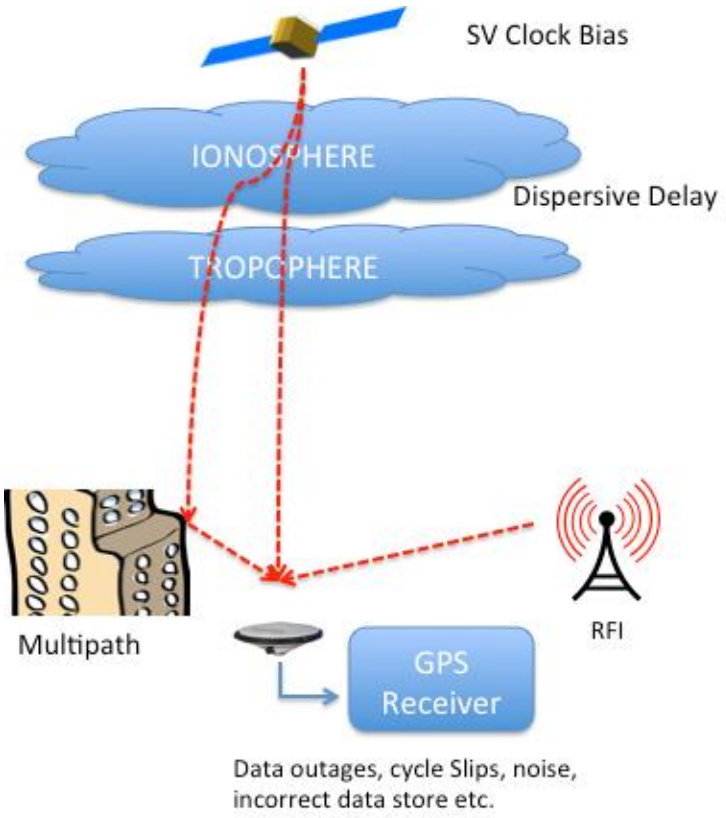

Figure 14. Error Sources pertinent to study of Ionosphere

The FAA WAAS program has funded several efforts on this front to generate what's referred to as "WAAS Supertruth Data" for development and testing of WAAS integrity algorithms. An equally powerful tool was developed by the FAA LAAS Program that was specifically designed to study and continuously monitor the ionospheric gradients between relatively short distances that can be threatening to GBAS. This software tool is called Long-Term Ionospheric Anomaly Monitoring (LTIAM). LTIAM was designed to estimate ionospheric delay precisely and was validated by comparing its results to the WAAS Supertruth solutions. .

LTIAM has been designed and developed to process the raw measurements generated by a network of dual-frequency GPS receivers and estimate some of the errors mentioned in the paragraphs above. Post estimation of the errors, the tool automatically generates potential threats to the GBAS caused by the ionosphere. Trained professionals then confirm these automatically generated potential threats manually. For the purpose of this effort, LTIAM will be used as the tool which has been validated and used by the FAA, as the method of processing data from the lower latitude GPS networks.

3.2 Days of Interest for threat processing

It is well known in the space weather community that Ionospheric inhomogeneity is a function of time of day, day of year, year within the 11-year solar cycle, and location on Earth.
There are several space weather parametric indicators that capture the state of the ionosphere over the Earth very effectively. Two such parameters are Kp and Dst. The geomagnetic index Kp is a global average of horizontal component of earth's magnetic field ranging between 0 and 9. The larger the Kp number the larger the strength of geomagnetic activity/storm. Disturbance, Storm-Time (Dst) is another measure of the geomagnetic disturbance, measured as the hourly averaged difference in nano-Tesla (nT) from the daily mean. Whereby, the lager deviation from the mean in Dst is indicative of the strength of the storm at any given location. For mid-latitude ionospheric study, both Kp and Dst are used to identify days to study potential ionospheric threats to GBAS.

Despite their effectiveness, both Kp and Dst fail to completely capture the subtle turbulences within the ionosphere for Southern Latitudes. Experts in this field at INPE and Boston College have suggested using the amplitude scintillation parameter S4 (in addition to Kp and Dst) to identify post-sunset ionospheric activities in Southern Latitude region. S4 is defined as:

$$S_4 = \left(\frac{\langle I^2 \rangle - \langle I \rangle^2}{\langle I \rangle^2} \right)^{1/2}$$

Where, I is the intensity of the signal and mathematical operator < > denote averaging.

Scintillation provides a measure of the fading of a given signal. At GPS frequency transmission, Scintillation causes loss of lock on the carrier tracking of the GPS signal causing cycle slips to the carrier phase measurement and complete loss of carrier and code tracking until eventually losing the entire GPS pseudorange measurement. The scintillation effect to an RF signal is generally caused by rapid fluctuations in the ionosphere as well as when the RF signal travels through the edges of the depletions. Scintillation impacts both the carrier phase and the code phase and can be measured and evaluated directly by those GPS receiver measurements.

Basu [10] captured this variability succinctly in his famous diagram describing signal fading / scintillation (as shown in Figure 15 below). This figure shows larger fading during post sunset time during both solar maximum and the solar minimum. The strength of the fading is higher during solar maximum as compared to benign solar activities.

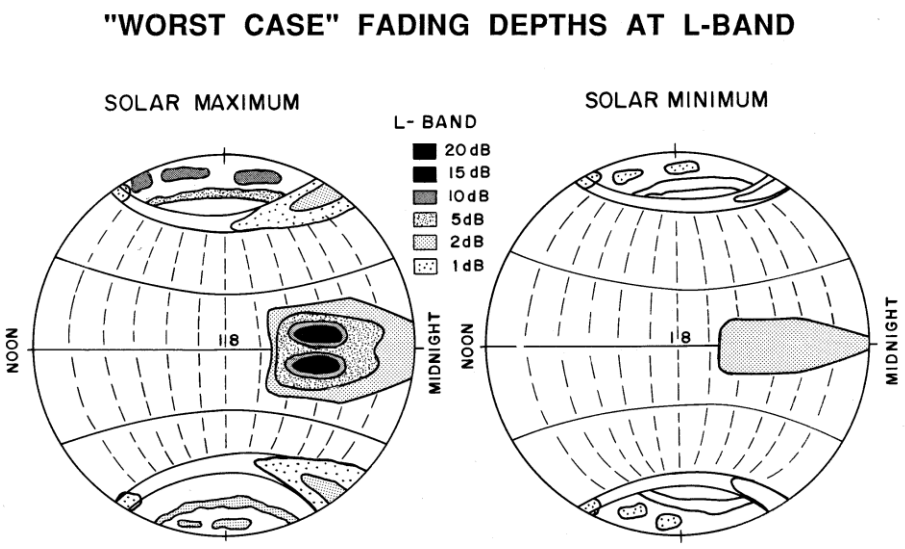

Figure 15. Fading Depth at L Band as a function of time and location [10]

The effect of temporal variability of ionospheric scintillation for one specific location in the southern hemisphere is captured by Doherty [10] in Figure 16 below. It shows the measured S4 at Cuiaba, Brazil from 2005 to 2013 clearly indicating larger scintillations during the current solar max and virtually no scintillation during current solar minima. These plots also indicate larger scintillations from October until April for the years of high solar activities.

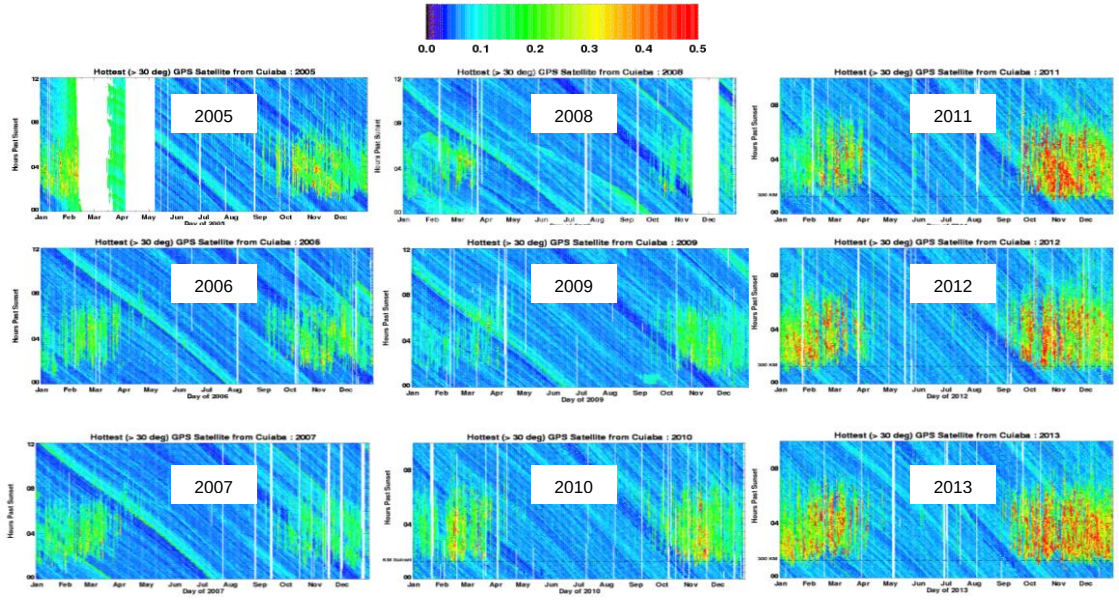

Figure 16. GPS Scintillation for current solar cycle for Cuiaba, Brazil [10]

Figure 17, (courtesy of Dr. Patricia Doherty of Boston College), show the daily variation in scintillation measurement at Dourados, Brazil for October 21-24, 2013. The chart clearly indicate that during a high solar cycle, during months of high ionospheric activities, the scintillations primarily occur during the post sunset hours.

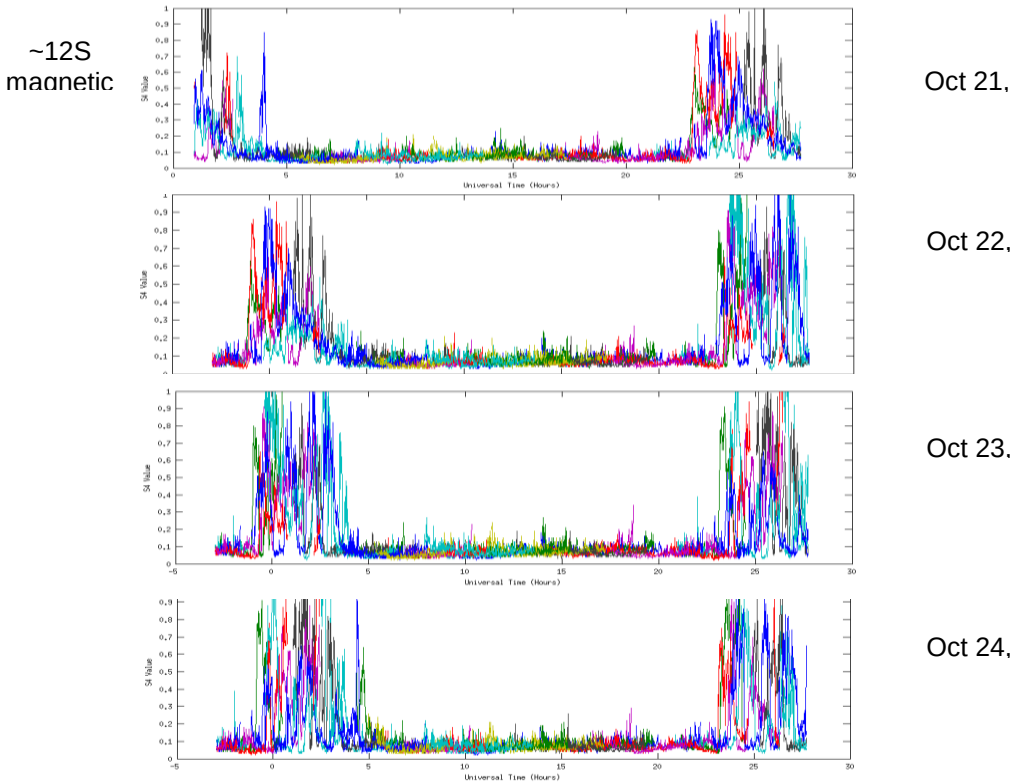

Figure 17. S4 variations during October 21-24, 2014 at Dourados, Brazil

Using dual-frequency data from several of the LISN and other stations in South America, the scientific research teams at INPE and Boston College used the Dst and S4 indices to identify 123 days (Over the last 3 years) to support development of the threat model for GBAS.

The dates we were identified as:

1. 8 non scintillating dates (as reference for the processing tool)
2. 85 scintillating days (based on depth of scintillation and number of satellites scintillating during the day at different locations within Brazil)
3. 7 storm days based on Kp index
4. 23 days of high geomagnetic activity (based on Dst)

Appendix A contains all the identified dates from 2011 until 2014.

Phase scintillation is yet another effect that can be exploited to identify days of interest for this processing. However, it was shown by Pradipta and Doherty [13] that the correlation between the

phase and amplitude scintillation is very high (as indicated in the plot below). Thus, negating the need to identify dates based on high phase scintillations. Figure 18 shows the correlation between phase and amplitude scintillation for several days in 2012 for SJ Dos Compos, Brazil.

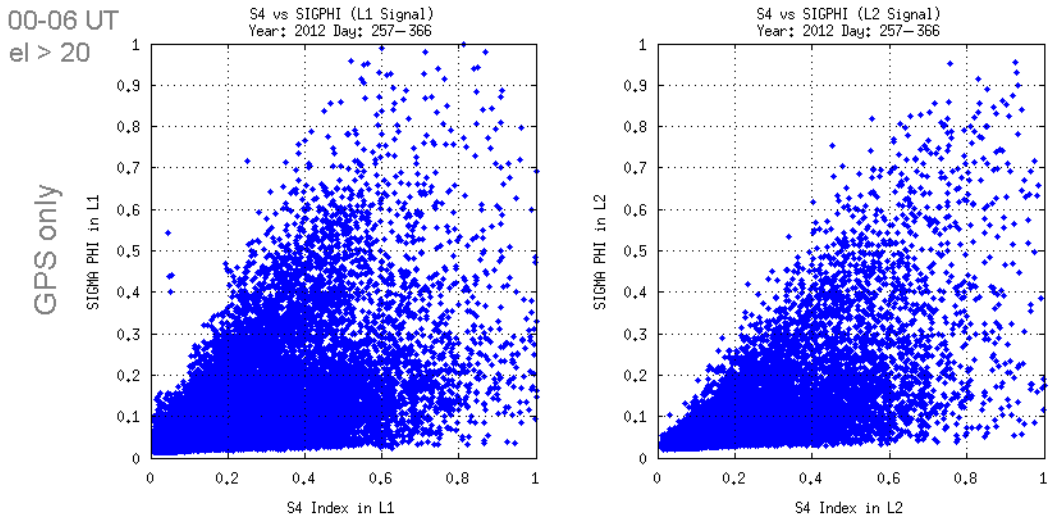

Figure 18. Correlation between Phase and Amplitude scintillation [13]

3.3 Available Data Sources

Before a comprehensive analysis of ionospheric gradients can be made using data from a given GPS network, the capacity of the network to detect the full range of likely gradients must be assessed. Two GPS stations observing the same satellite are used to detect spatial ionospheric gradients, such that the inter-station spacing and azimuth dictates the ability of that station pair to detect a gradient. Likewise, the distribution of inter-station spacing and azimuths within a network dictates the capacity of that network to detect gradients. Detection of large ionospheric gradients over short distances requires a relatively dense GPS network with a wide range of short baselines and inter-station azimuths. Figure 19 shows the locations of the dual-frequency data collection network that was used for the purpose of developing the threat model.

RBMC

RBMC, Brazilian Network for Continuous Monitoring of GNSS Systems, currently consists of more than 100 data collection stations. Each station contains a dual-frequency receiver located at a precisely surveyed location collecting GPS and GLONASS data at one sample every 30 seconds. These stations are networked and the data is continually provided in Rinex 2 format at the IBGE FTP-site (on a daily basis). More information about the specific installation, types of antenna and receivers can be found on the Brazilian Institute of Geography and Statistics (IBGE) web page (http://www.ibge.gov.br/english/).

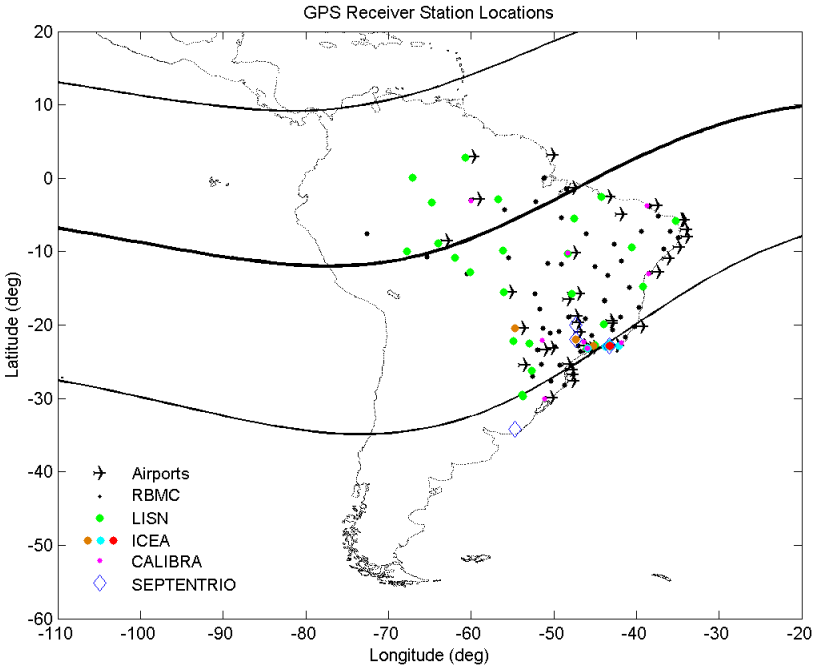

Figure 19. Available Data Collection Network in Brazil

LISN

Low-Latitude Ionospheric Sensor Network (LISN) is currently in the process of being installed in the South American region to study the low latitude ionosphere and upper atmosphere. The LISN distributed observatory will eventually be comprised of nearly 70 GPS receivers with the capability to measure Total Electron Content (TEC), amplitude and phase scintillation and Traveling Ionospheric Disturbances (TIDs). The LISN network will include 5 ionosondes able to measure nighttime E-region densities and 5 collocated magnetometers that will be placed along the same magnetic meridian. For the purposes of GBAS threat model analysis, dual frequency data from the relevant LISN sites was provided by Boston College (BC).

ICEA/SIPEG/CIGALA

There are other networks of dual-frequency GPS receivers within Brazil that are owned and operated by Instituto de Controle do Espaço Aéreo (ICEA), Instituto Nacional da Propriedade Industrial (INPE), and the Universities. Dual-frequency data from these different network sites was provided by the members of Departamento de Controle do Espaço Aéreo (DECEA) and ICEA.

These networks include:

1) Integrated Positioning System for Geodynamic Studies (SIPEG) network operated by INPE
2) Concept for Ionospheric scintillation mitiGAtion for professional GNSS in Latin America (CIGALA) network operated by a consortium. The goal of this effort is to understand the cause and implication of ionospheric scintillation disturbances at low latitude, model their effects, and develop mitigations.
3) ICEA operated network of dual frequency receivers (Trimble and Septentrio) to observe effects of the Ionosphere on the GNSS signal during the present peak in solar activity.

In all, there is information available from more than 180 reference stations spread across Brazil. Despite unavailability of data (due to unknown reasons) from some of the network stations, for any given selected day for data analysis, the analyst team had access to uncorrupted dual-frequency information from more than 110-120 stations (on average). Figure 20 shows the baseline distance histogram from all potentially available reference stations within Brazil. It shows a histogram of number of stations that have relative baseline of less than 100 Km. For the purpose of this analysis, there are 135 station pairs that have a baseline of less than 100 Km. Out of these, 66 of those station pairs have a baseline of less than 20 Km. Considering just the inter-station spacing, the threshold (minimum) 2-station separation required to detect a given ionospheric gradient, for a range of maximal ionospheric delays assumes the maximal ionospheric gradient is parallel to the inter-station azimuth. The 'maximum gradient' detectable by a network is effectively the saturation level of the detection technique for that network. An ionospheric gradient of magnitude greater than the maximum detection level will be underestimated by the network.

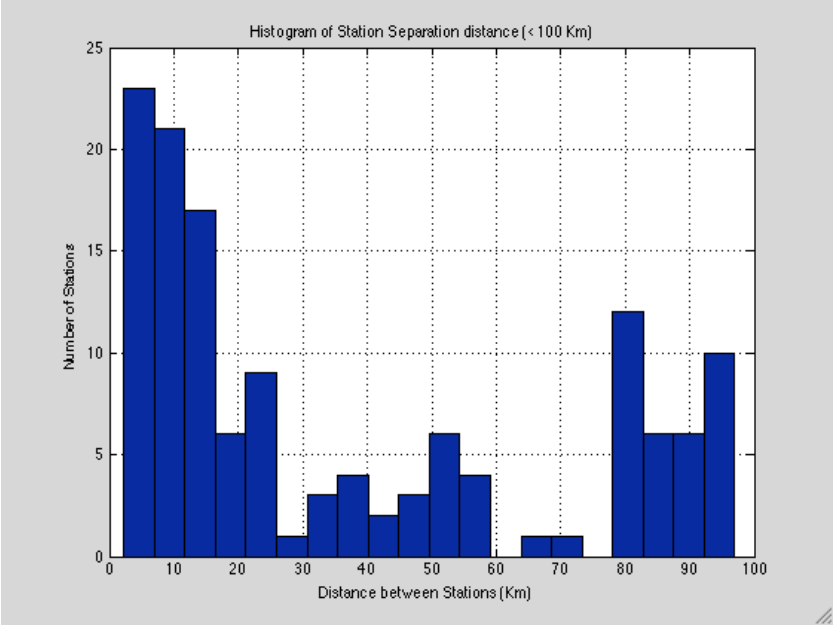

Figure 20. Histogram of station pair baselines (<100 Km)

Even though the smaller baselines are not uniformly distributed across the Brazilian airspace, there is sufficient coverage over different geomagnetic latitudes for the results to be relevant for the Brazilian airspace. See Figures 21 and 22 below for the distribution of baseline's below 100 Km. The red dots across the map indicates the presence of a baseline below 100 Km.

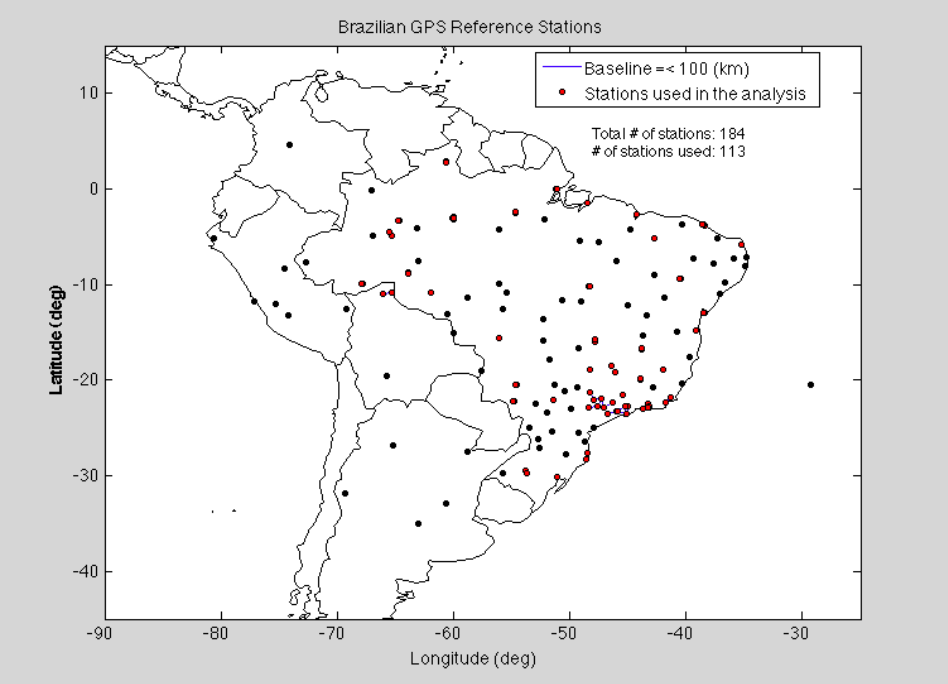

Figure 21 and 22. Receiver baselines in the area near Rio de Janeiro.

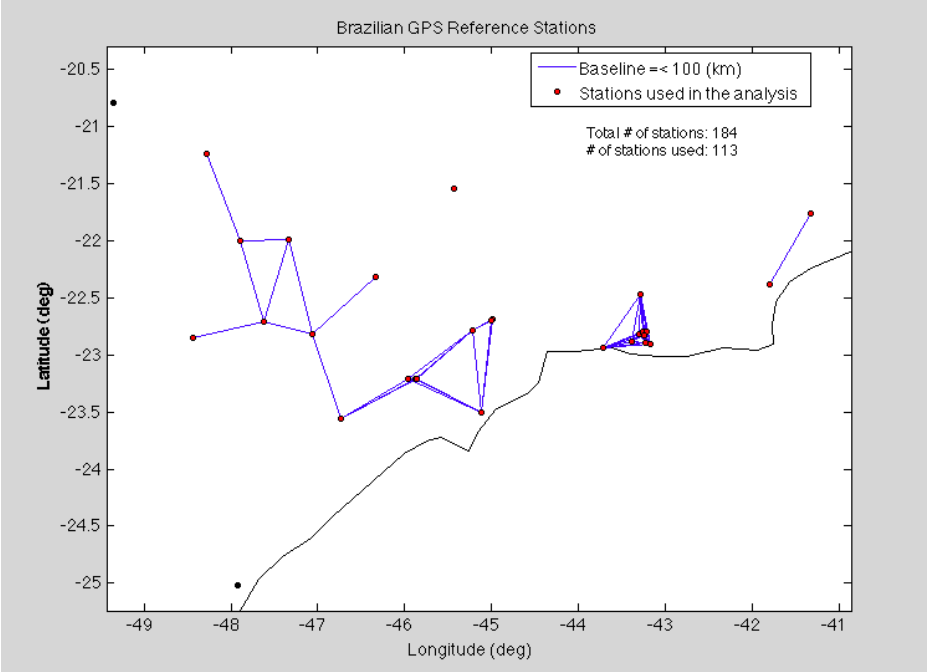

Structure of FTP Server Directory for Brazilian Data

As data was gathered and validated it was formatted and posted on the Mirus website so that the data analysis team could access the data with the LTIAM tool for analysis. The directory for Brazilian data on the MIRUS FTP server is structured first by year, and then day of year as shown in Figure 23. Each sub-folder (default_directory/yyyy/doy) consists of a RINEX data folder, a GPS navigation data folder, and an IONEX data folder. Each component is described as below.

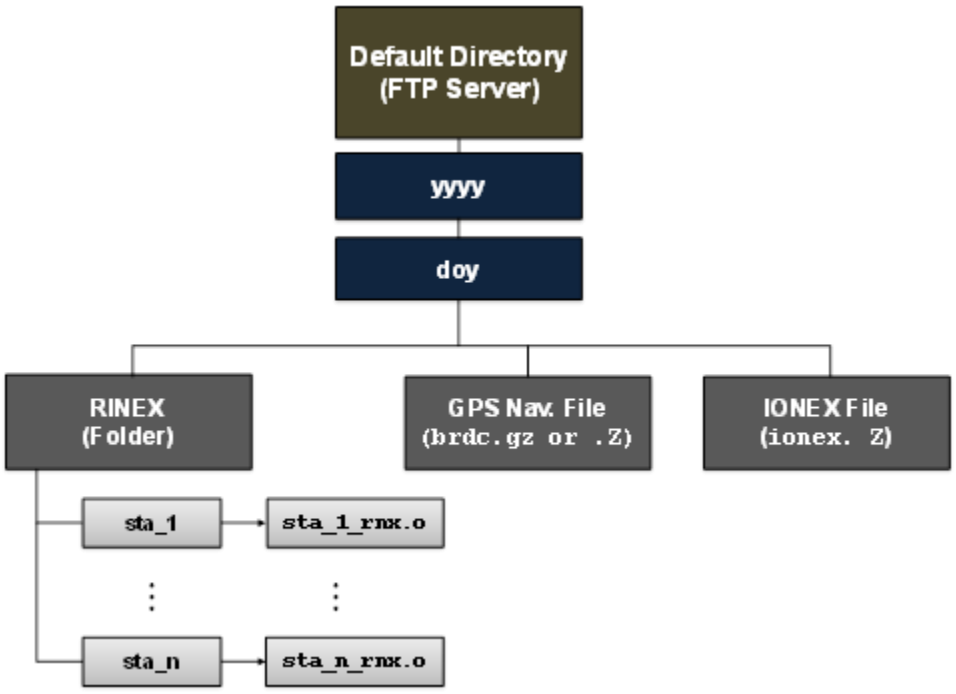

Figure 23. Directory Tree

1. RINEX data

Example: “default_directory/yyyy/doy/rinex/sta_name/rinex_file.o”

As shown in the example above, RINEX files for each station is stored in sta_name/, and is in the observation data format (.o).

2. GPS navigation data (brdc file)

Example: “default_directory/yyyy/doy/brdcdoy0.yyn.gz”

As shown in the example above, a GPS navigation file is directly stored in doy/, and is in the compressed file format (.gz). As an example, the file name could be 'brdc1030.08n.gz'.

3. IONEX data

Example: "default_directory/yyyy/doy/igsgdoy0.yyi.Z"

As shown in the example above, an IONEX file is directly stored in doy/, and is in the compressed file format (.Z). As an example, the file name could be 'igsg1030.08i.Z'.

3.4 LTIAM

The FAA in assistance from NAVTAC and Korea Advanced Institute of Science and Technology (KAIST) has developed the Long-Term Ionospheric Anomaly (LTIA) monitoring tool to support Ground-Based Augmentation Systems (GBAS). This tool is used to build an ionospheric anomaly threat model, evaluate its validity over the life cycle of the system, continuously monitor ionospheric anomalies, and update the threat model if necessary. The tool is currently being used for continual validation of the ionospheric threat model for GBAS in CONUS. The tool is designed to read the data files generated by the CORS network of receivers and identify potential anomalous behavior of the ionosphere for GBAS. One point to reiterate here is that LTIAM tool is validated against the processing functions that generate the WAAS Supertruth data; in terms of LTIAMs assessment and estimation of various error sources.

LTIA Monitor Overview

The LTIA Monitor is composed of two main modules: Ionospheric Event Search and GPS Data Process. The first module checks the potential occurrence of an ionospheric storm on a given day based on space weather indices. The second module derives ionospheric delay and gradient estimates, and generates ionospheric anomaly candidates. These two modules can work separately, and the full operation of the LITA Monitor can be performed by combining them. Submodules that compose each main module are also independently executable programs. Figure 24 below shows a flowchart of the LTIA Monitor that consists of main programs (orange) and input/output files (green).

The programs operate automatically in series. When necessary, users can execute individual programs and scripts separately given that all of the input elements are well equipped. The GPS Data Process module is divided into three sub-modules. The first sub-module, Data Download, constructs the information of GPS stations and gathers data in Receiver Independent Exchange (RINEX) format. This sub-module can be extended to include any other network stations depending on the user's purpose. Currently the LTIA Monitor collects data from the CORS

network on CONUS only. The second sub-module, Ionospheric Delay Estimation, derives ionospheric delay estimates from the data that was obtained from Data Download. Ionospheric anomaly candidates are selected in the last sub-module, Ionospheric Anomaly Candidate Screening. The following convention is adopted to avoid any confusion between different entities: italics for functions or scripts, underlining for MATLAB variables, bold for file types, and courier for file names and directories. The name of a file produced in the GPS Data Process is defined by the information of data, which includes the marker ID of a station (ssss), 4-digit year (yyyy), and day of year (ddd). M-files (*.m) in MATLAB are expressed by omitting the extension m for the case of functions. The tool was modified slightly to read Rinex 2 files or Compressed Rinex files from various networks of stations in the Brazilian airspace (refer to the previous section of this document) and generate a list of potential GBAS threats for the Brazilian airspace. Please refer to the LTIAM user manual [16] to gain a more complete internal understanding of the tool. Validated processing algorithms of the tool have remained unchanged.

Once the raw measurements are input into LTIAM, the tool automatically begins characterizing each station for its internal corrections and then generating potential pairs for investigation of the GBAS threat. This selection of station pairs is driven by choosing the max distance between station pair – in the configuration of the tool for a given application. Once the station pairs are generated, the tool inherently detects the station pair's that may potentially have gradient larger than 200 mm/Km (another parameter set within the tool). After this, LTIAM automatically eliminates the gradients based on certain sanity checks – parameters for which are also set in the configuration file for the tool. Following this process, the tool generates a list of potential threats that requires manual investigation to screen as valid or invalid threats.

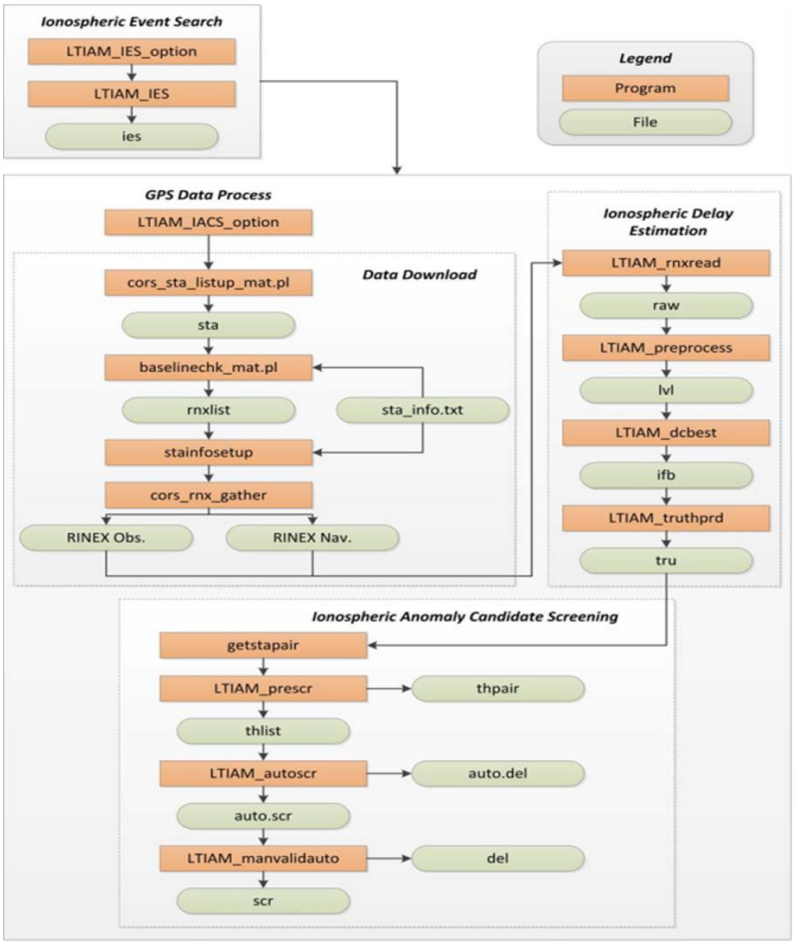

Figure 24. LTIAM Flow Chart [16]

Example of summary page generated by the tool.

```
###
### Statistics of Long-Term Iono. Anomaly on 2013 - 317
###

 # of stations        : 43
 # of station pairs    : 39
 # of SVs             : 31

1. Pre-screening
 # of station pairs of pre-candidates : 4
 # of pre-candidates    : 56

2. Auto-screening
 # of discarded candidates  : 45
 # of remaining candidates  : 11

3. Automated manual validation
 # of discarded candidates  : 5
 # of remaining candidates  : 6
```

The example above depicts how the LTIAM tool identifies significant ionospheric events amidst other errors that the receiver captures within the actual signal. This helps shape the boundaries of the threat model. The summary report shows the number of automatically discarded candidates and the final remaining candidates that require manual investigation. The tool also provides the user with exact station pairs and the satellite PRN to perform manual investigation.

The primary task of manual investigation/validation is to ensure that the indicated gradient between the identified station pair and the satellite is indeed induced by the ionospheric activity rather than the other error sources as discussed previously. This task is accomplished by observing the ionosphere estimation using dual frequency measurements between the two stations (I_{phi}) and then comparing it with the gradient measured using only L1 code minus carrier (I_{CMC}). If these two estimates show variability in tandem, it can be reasonably assumed that; at the instance where there is complete correlation between these two estimates; is due to ionospheric activity.

3.4.1 An Example

- DoY 317 Year 2013.
- Data Input – Rinex Files from RBMC and LISN networks
- Number of pre-candidates generated by LTIAM are: 56
- Auto-screened (discarded) candidates: 51
- Number of candidates to be manually investigated: 6

Once the generation of potential candidates is complete, the tool provides the user with a short list of candidate pairs (station pairs and SV number) for manual screening. The tool also provides manual diagnostic capability to study the measurements from any station pairs and for all SVs visible to those station pairs. One such diagnostic plot is shown in Figure 25 below.

The figure on the top left (Figure 25) shows the slant ionopheric delay as measured from each stations (in this case its SAVO and SSA1 from RBMC which are separated by 10 Km) for a particular satellite (in this case SV#12). The top right plot shows the ionospheric slope experienced between the two stations. The bottom left plot is the SV elevation observed by each station. The plot on the bottom right shows the dual frequency ionospheric estimate (I_{Φ}) of the slope between the stations and the single frequency code-minus-carrier ionosphere estimate (I_{CMC}) of the slope.

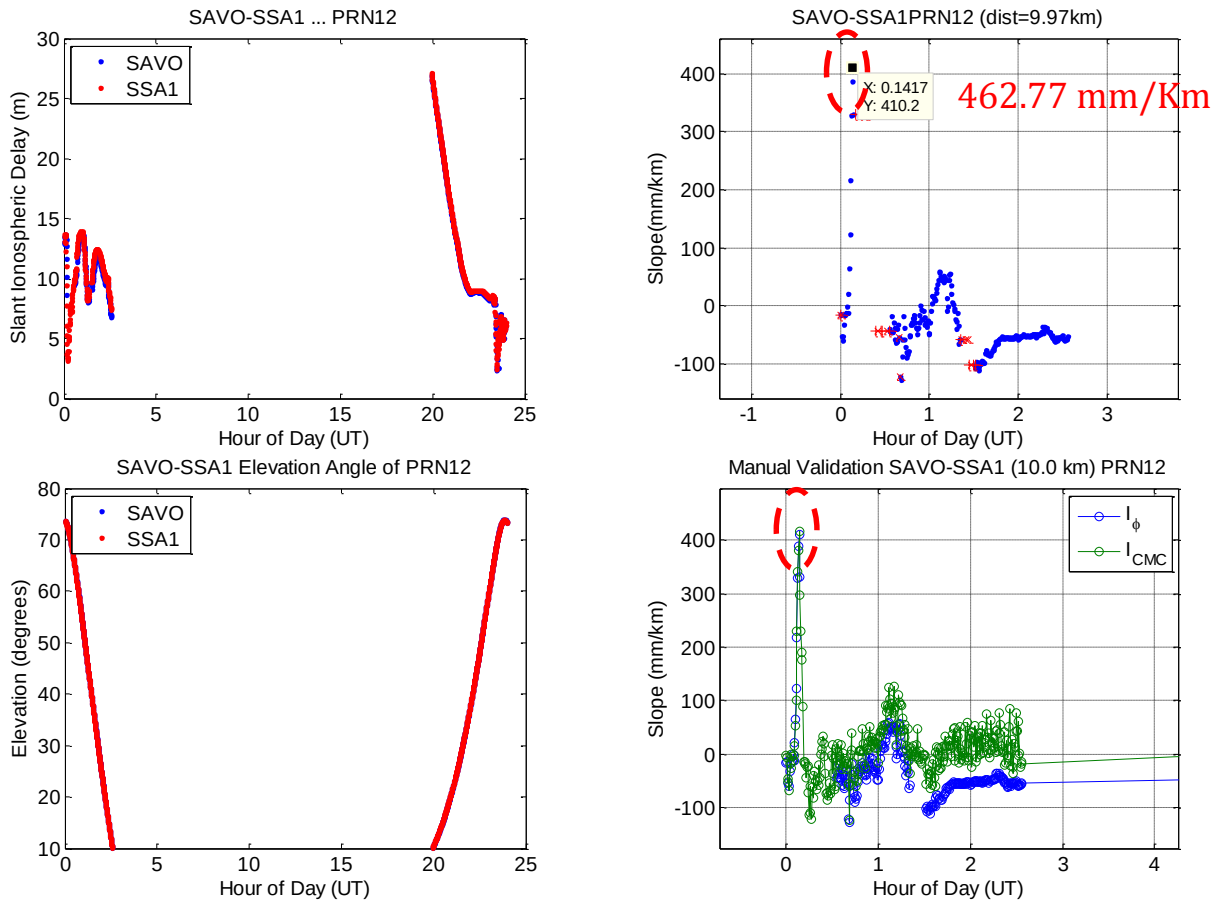

Figure 25. Manual diagnostic plots generated by LTIAM

Concluding from the plots above, we can observe that shortly after midnight (UT), a larger variation in both estimates of the ionospheric delays occurs. This clearly indicates an ionospheric feature rather than a footprint of any other sources of errors (discussed in previous sections). The slopes are measured for this instance and noted as a point to generate the threat model.

3.5 GBAS Ionospheric Threat Model for Low-Latitude

As noted in previous sections, the Category I GBAS cannot fully detect and mitigate complete range of ionospheric threats. It is important to first define the characteristics of the ionosphere and then determine the bounds of the defined characteristics. The CONUS threat model is defined as the observed gradient as a function of satellite elevations. This threat model is further defined using constrains on front width, velocity, and differential delay.

For the Brazilian threat model, the same assumptions as the CONUS is made where the threat space is constrained using maximum observed gradients against the satellite elevation angles and similar constrains on the front width, velocity, and differential delay. The threat space has been determined by using empirical data collected during the current solar cycle using methodologies

described in the sections above. At the behest of the contributing scientists from INPE, two additional pieces of information are generated during the identification of the worst observed gradient – that is the exact time of occurrence of the gradient and the orientation of the station pair (with respect to true North) that observed the gradient.

Figure 26 below shows the observed gradients with respect to the elevation of the satellites for all stations-satellite pairs. The figure clearly shows gradients over the CONUS threat model (shown in blue). The highest gradient observed is 850.7 mm/Km observed near Sao Jose Dos Campos between the station pair SJCU (CIGALA) and SJSP (RBMC) on March 1, 2014 on SV 11.

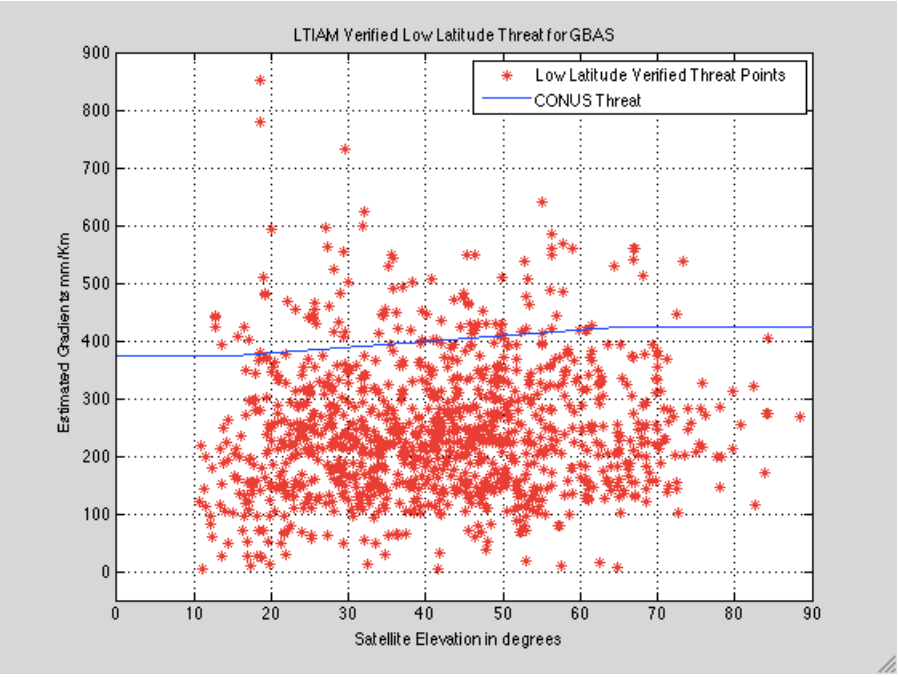

Figure 26

The table below contains the list of all significant gradients observed in the data.

DOY-YYYY	Sta #1	Sta #2	Dist. (km)	Az. of Stations (deg)	PRN	Hour UT (decimal)	Slope (mm/km)	El. (deg)
060-2014	SJCU	sjsp	9.72	267.723	3	1.067	850.7	18.604
060-2014	SJCE	SJCU	9.92	268.041	3	1.071	779.6	18.62
322-2013	lsjk	SJCU	9.90	268.071	22	2.0080	732.2	29.65
314-2013	savo	ssa1	9.97	246.496	18	1.9580	641.2	55.06

066-2014	riod	BAAF	10.49	228.890	11	2.8420	638.5	32.058
310-2013	savo	ssa1	9.97	246.496	18	1.1920	596.4	27.091
055-2014	savo	ssa1	9.97	246.496	3	1.2210	562.6	27.332
056-2014	savo	ssa1	9.97	246.496	27	1.0920	553.3	29.278
319-2013	savo	ssa1	9.97	246.496	24	22.8500	548.0	46.381
326-2013	sjsp	SJCU	9.72	267.723	21	0.7833	538.5	52.873
065-2014	savo	ssa1	9.97	246.496	11	2.3290	510.2	49.926
365-2013	savo	ssa1	9.97	246.496	21	23.8600	501.2	38.250
056-2014	ceft	FORT	12.22	252.212	32	2.1750	500.5	29.987

Table 2. Observed significant gradients.

Figure 27 below shows the time of occurrence of all identified gradients.

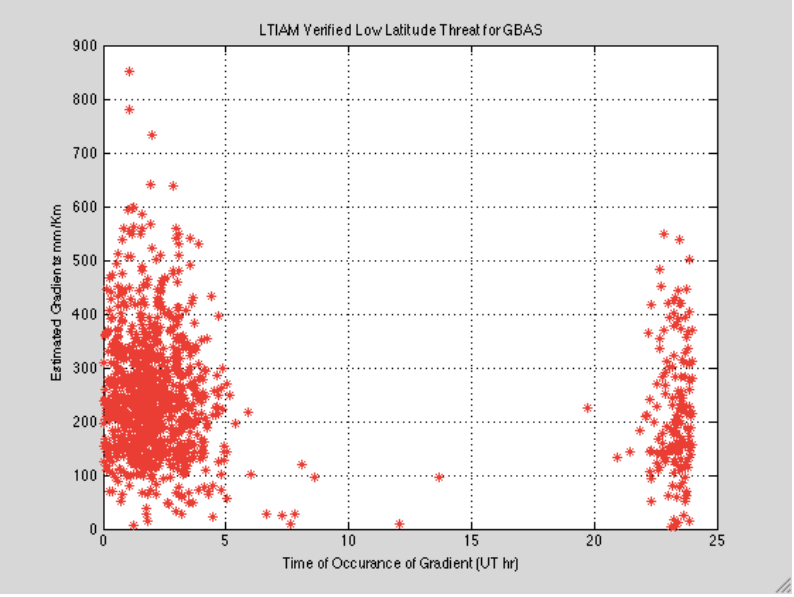

Figure 27

Figure 28 below shows the orientation of the station pairs from which the threatening GBAS gradients were observed. The figure clearly shows that the station pairs that are orientated in NE-SW direction at 250 degrees from true North or 75 degrees with respect to True North; observed most of the highest gradients.

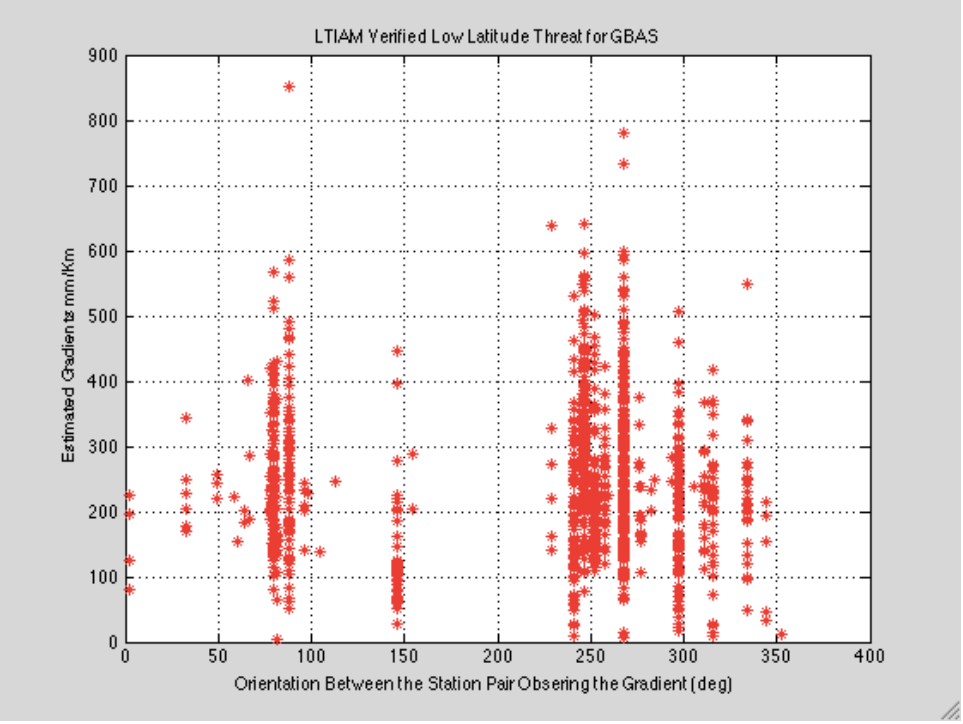

Figure 28. Station pair orientation

Observations:

1. As suspected, the ionosphere over the Brazilian airspace is very active as compared to CONUS. Out of all the active days processed so far, it is clear that gradients between two reference stations far exceed the CONUS threat model frequently. The larger gradients are not location dependent, they are close to Sao Jose Dos Campos, Rio Di Janeiro, and Salvador.

2. All of the significant gradients are observed during the post sunset hours – between 2100 and 0500 (UT) and predominance of those gradients occurred between 0000 – 0400 (UT). The timing of these gradients during post sunset hours overlaps with the occurrence of recorded scintillations on the L-band. Further, during the analysis of the data using LTIAM, it is clear by observing slant ionosphere delay variations that the ionospheric is not a wedge shaped as assumed during CONUS storm. Instead, they are more shaped as depletions of varied width, one following the other.

3. Additionally, these large gradients are detected by the station pairs that are oriented in the Northeast and Southwest direction indicating the movement of the depletions in the West to East direction. Figure 29 below shows the magnetic declination for South American continent. These declination lines vary over time. Recent specific magnetic declination for

Rio de Janeiro and Salvador are close to -22 degrees. Thus, any stations with true North orientation of 68 degrees or 248 degrees will be along the magnetic lines for those locations.

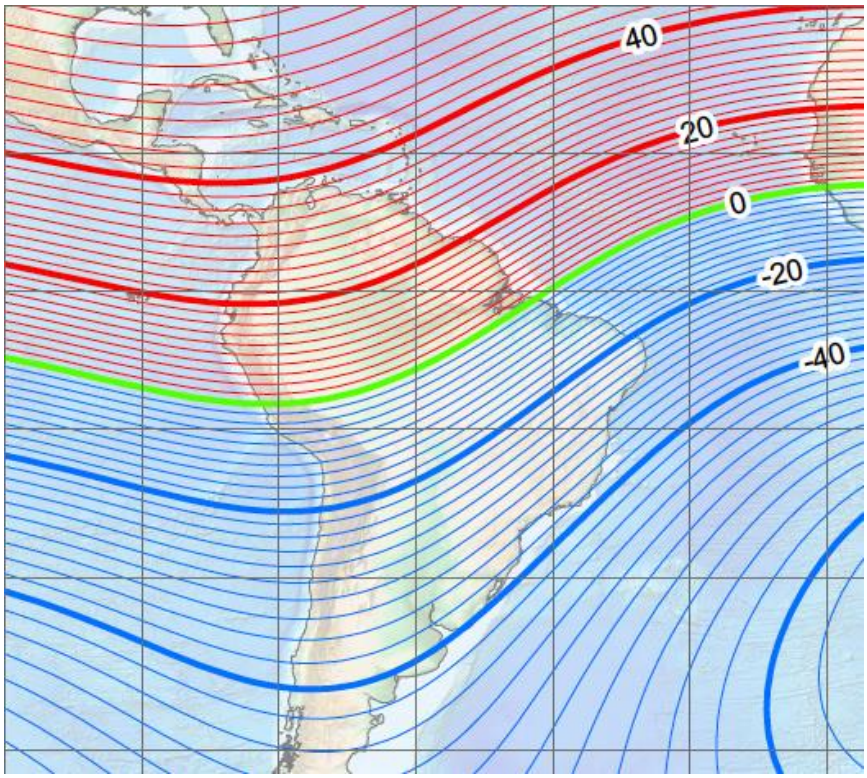

Figure 29. Magnetic declination for South America

This is consistent with the orientations of the stations pairs that observed threatening gradients for GBAS – which are close to 250 degrees and 70 degrees (True North).

4. No threatening gradients were found during daytime (0900 – 2100 UT). This not to indicate that there were no gradients during daytime. However, the LTIAM is configured to detect gradients above 200 mm/Km and no gradients were flagged during the daytime by LTIAM.

4 Conclusions & Recommendations

The Ionospheric behavior over the Brazilian airspace was studied for the current Solar Cycle #24. Instead of evaluating all the data, about 120 days were chosen based on the space-weather indices and measured L band Scintillation. The number of days was selected to be more than 100 to ensure detection of threatening gradients in spite of data un-availability or other hardware failures. Dual-Frequency GPS Data was gathered from several networks (RBMC, LISN, CIGALA, SIPEG, and ICEA) for those specific days and processed through LTIAM.

The process of generating the threat model was similar to the one followed by the FAA to generate the ionospheric threat in CONUS. For each day of data processing, the highest gradient was searched for all applicable station pairs and the SV. These gradients were documented along with the time of occurrence, elevation of the SV, and the orientation of the station pairs.

It is found that the CONUS GBAS Ionospheric threat model is insufficient in capturing the threats offered by the Ionosphere over Brazil. The gradients exceeded 500mm/Km frequently and >600 mm/Km occasionally. All of the captured threatening gradients occurred post sunset and a careful analysis showed that Enhanced Plasma Bubbles caused most observed gradients. It is also shown that the highest scintillation occurred during the same time period of heightened gradient detectability, which indicates a correlation between these two phenomenon. The space weather scientific community is still unclear if the onset of L band scintillation always implies presence of depletion bubbles.

Yet another observation that supports the assertion that most detected GBAS Iono threat gradients were induced by plasma bubbles is the fact that most all of these threatening points were observed by the station pairs oriented along the magnetic force lines. It is well known that post-sunset depletions do travel West to East along the magnetic lines of force hence most of the stations pairs oriented perpendicular to this direction (such as ONRJ and RIOD near Rio de Janeiro) do not detect the presence of inter-station ionosphere gradients.

Recommendations

1. It is recommended that a program of ongoing monitoring of ionospheric gradients be considered to ensure that the parameters of the GBAS ionospheric threat model remain representative of the ionospheric conditions experienced in South America. There is a real need for short-baseline GPS network observations throughout the region where currently very little short-baseline data is available. It is recommended that this program be established immediately.

2. To evaluate the system performance using the new threat model, the parameters of the GBAS threat model (width and speed of plasma bubble and maximum differential delay) should be

reviewed and verified. Findings from this effort must be incorporated into the Block II upgrade. In particular, the finding of a maximum ionospheric gradient of >800 mm/km, well above the upper boundary of the certified threat model (395-412mm/km) must be considered and handled appropriately.

3. Most threatening gradients occurred in conjunction with Scintillation. It has been asserted in the past that the scintillation observed on L band are precipitated at the edges of the depletions. However, there is no documented study that correlates the strength of scintillation to the depth of the observed short-baseline gradients. This correlation can be highly useful in establishing bounds on the threats to the GBAS ground system. It is recommended that additional study be accomplished to ascertain whether quantifiable correlation between scintillation and gradients exists.

5 References

[1] FAA-E-3017, "Specification for Non Federal Navigation Facility, Category I Local Area Augmentation System, Ground Facility", September 29, 2009.

[2] ICAO Standards and Recommended Practices, Annex 10, Vol I, Radio Navigational Aids, July 2006.

[3] RTCA, Incorporated. (2001). Minimum operational performance standards for global positioning system/local area augmentation system airborne equipment (RTCA/DO-253A). Washington, DC: RTCA, Incorporated.

[4] RTCA, Incorporated. (2001). GNSS based precision approach local area augmentation system (LAAS) signal-in-space interface control document (RTCA/DO-246B). Washington, DC: RTCA, Incorporated.

[5] S. Jung and J. Lee, "Long Term Ionospheric Anomaly Monitoring for Ground Based Augmentation Systems." *Radio Sci*., 47, RS4006, July 2012, doi:10.1029/2012RS005016.

[6] J. Lee, S. Jung, M. Kim, J. Seo, S. Pullen, and S. Close, "Results from Automated Ionospheric Data Analysis for Ground-Based Augmentation Systems," *Proceedings of the Institute of Navigation International Technical Meeting* (ION ITM 2012), Newport Beach CA, January, 2012

[7] J. Lee, S. Jung, and S. Pullen, "Enhancements of Long Term Ionospheric Anomalies Monitoring for the Ground-Based Augmentation System," *Proceedings of the Institute of Navigation International Technical Meeting* (ION ITM 2011), San Diego, CA, January 24-26, 2011

[8] J. Lee, S. Jung, E. Bang, S. Pullen, and P. Enge, "Long Term Monitoring of Ionospheric Anomalies to Support the Local Area Augmentation System," *Proceedings of the 23rd International Technical Meeting of the Satellite Division of the Institute of Navigation* (ION-GNSS 2010), Portland, OR, September 2010.

[9] Basu, Sa., and Basu, Su., "Equatorial scintillation – A Review", J. Atmos. Terr. Physics, 1981.

[10] Doherty Patricia et al, "Characterization of the Ionosphere over the Brazilian Airspace", presentation made to DECEA and INPE at Sao Jose dos Campos, March 10, 2013.

[11] De Paula et al, "Magnetic conjugate point observations of kilometer and hundred meter scale irregularities and zonal drifts", Journal of Geophysical Research, Vol. 115, 2010.

[12] Pullen Sam, several personal communications (2014).

[13] Pradipta R. and Doherty Pat, "Characterizing Correlation between Amplitude and Phase Scintillation", Presentation during Data Analysis Working Group (DAWG), August 2014.

[14] L. C. Gentile, W. J. Burke, and F. J. Rich, "A global climatology for equatorial plasma bubbles in the topside ionosphere", Annales Geophysicae, 24, 163–172, 2006.

[15] Pullen et al, "The Impact and Mitigation of Ionosphere Anomalies on Ground-Based Augmentation of GNSS", Proceeding of IES 2008. http://waas.stanford.edu/papers/PullenIES08.pdf

[16] FAA (2011). Long-Term Ionospheric Anomaly (LTIA) Monitor of the Local Area Augmentation System (LAAS), Version 1.2, November 2011.

Appendices

Appendix A – Selected Days for Threat Assessment

	DOY
Non-Scintillation Days:	(8 Days)
4/18/2012	109
4/19/2012	110
4/20/2012	111
6/15/2012	167
6/16/2012	168
9/17/2012	261
9/18/2012	262
9/19/2012	263
Storm Days:	(7 Days)
6/1/2013	152
6/28/2013	179
6/29/2013	180
10/2/2013	275
2/19/2014	50
2/20/2014	51
2/27/2014	58
Scintillation Days:	(85 Days)
11/6/2013	310
11/7/2013	311
11/8/2013	312
11/9/2013	313
11/10/2013	314
11/11/2013	315
11/12/2013	316
11/13/2013	317
11/14/2013	318
11/15/2013	319
11/16/2013	320
11/17/2013	321
11/18/2013	322

11/19/2013	323
11/20/2013	324
11/21/2013	325
11/22/2013	326
12/1/2013	335
12/2/2013	336
12/3/2013	337
12/4/2013	338
12/5/2013	339
12/16/2013	350
12/17/2013	351
12/18/2013	352
12/19/2013	353
12/20/2013	354
12/21/2013	355
12/22/2013	356
12/23/2013	357
12/24/2013	358
12/25/2013	359
12/26/2013	360
12/31/2013	365
1/3/2014	3
1/4/2014	4
1/5/2014	5
1/6/2014	6
1/7/2014	7
1/8/2014	8
1/9/2014	9
1/10/2014	10
1/11/2014	11
1/14/2014	14
1/15/2014	15
1/16/2014	16
1/17/2014	17
1/18/2014	18
1/19/2014	19
1/20/2014	20
1/21/2014	21
1/22/2014	22

1/23/2014	23
1/24/2014	24
1/25/2014	25
1/26/2014	26
1/27/2014	27
1/28/2014	28
1/29/2014	29
1/30/2014	30
1/31/2014	31
2/1/2014	32
2/2/2014	33
2/3/2014	34
2/4/2014	35
2/5/2014	36
2/6/2014	37
2/11/2014	42
2/12/2014	43
2/13/2014	44
2/14/2014	45
2/15/2014	46
2/24/2014	55
2/25/2014	56
2/26/2014	57
3/1/2014	60
3/2/2014	61
3/3/2014	62
3/4/2014	63
3/5/2014	64
3/6/2014	65
3/7/2014	66
3/8/2014	67
3/27/2014	86
3/28/2014	87
Storm Days Identified by ICEA	**(23 Days)**
4/12/2014	102
7/14/2013	195
7/6/2013	187

6/7/2013	158
3/17/2013	76
11/14/2012	319
10/13/2012	287
10/9/2012	282
10/8/2012	281
10/1/2012	275
7/15/2012	197
4/24/2012	115
3/9/2012	69
3/7/2012	67
1/25/2012	25
10/25/2011	298
9/27/2011	270
9/17/2011	260
8/6/2011	218
5/28/2011	148
3/11/2011	70
3/1/2011	60

Appendix B. Brazil Station Master List

Station ID	Latitude	Longitude	Height	Network
alar	-9.749222755	-36.6534195	266.216	RBMC
amco	-4.87198782	-65.33397675	75.883	RBMC
amhu	-7.503245354	-63.02851486	68.946	RBMC
amte	-3.34568882	-64.70664978	45.784	RBMC
apsa	-0.060256001	-51.16746903	-11.06	RBMC
babr	-12.15004158	-44.99489594	443.054	RBMC
bail	-14.7966013	-39.17238617	44.685	RBMC
bair	-11.30564594	-41.85852051	723.913	RBMC
batf	-17.55487061	-39.74334335	108.848	RBMC
bavc	-14.88831043	-40.80270386	875.187	RBMC
bele	-1.408793807	-48.46255112	9.064	RBMC
boav	2.845183849	-60.70111466	69.494	RBMC
bomj	-13.25555706	-43.42173386	419.401	RBMC
braz	-15.94747353	-47.87786865	1106.009	RBMC
brft	-3.877445698	-38.42553711	21.673	RBMC
ceeu	-3.877547264	-38.42554092	21.732	RBMC
cefe	-20.31079292	-40.31945419	14.292	RBMC
ceft	-3.710810184	-38.47291946	4.902	RBMC
cesb	-3.681268215	-40.33748627	56.818	RBMC
chpi	-22.68714523	-44.98515701	617.407	RBMC
crat	-7.238017082	-39.41560745	436.031	RBMC
cruz	-7.611161232	-72.67211151	235.987	RBMC
cuib	-15.55526161	-56.06986618	237.441	RBMC
eesc	-22.00494766	-47.89918137	824.556	RBMC
gogy	-16.66472626	-49.254673	734.194	RBMC
goja	-17.88327789	-51.72610855	755.3	RBMC
gva1	-18.85560608	-41.95761871	178.565	RBMC
gval	-18.85560608	-41.95761871	178.641	RBMC
ilha	-20.42778397	-51.34338379	375.019	RBMC
imbt	-28.23483849	-48.65572357	31.351	RBMC
impz	-5.491764545	-47.49723434	104.976	RBMC
maba	-5.362377167	-49.12229919	79.808	RBMC
mabb	-4.240957737	-44.81572342	6.58	RBMC
mabs	-7.533813477	-46.03971863	226.89	RBMC
mapa	-0.046687279	-51.09733582	-4.261	RBMC
mcl1	-16.72039414	-43.88131714	656.468	RBMC
mcla	-16.72039414	-43.88131714	656.539	RBMC

mgbh	-19.94189835	-43.92489624	974.832	RBMC
mgin	-22.31855965	-46.32802582	883.679	RBMC
mgmc	-16.71639061	-43.85831833	618.159	RBMC
mgrp	-19.20985985	-46.1325531	1123.465	RBMC
mgub	-18.91916084	-48.25605011	869.214	RBMC
mgv1	-21.54262161	-45.43499374	957.176	RBMC
mgva	-21.54262161	-45.43499374	957.208	RBMC
mscg	-20.4408989	-54.54070282	676.453	RBMC
msco	-19.00352097	-57.63698196	156.749	RBMC
msdo	-22.2168541	-54.81391144	467.843	RBMC
msdr	-22.19410515	-54.93040085	478.564	RBMC
mtba	-15.88996983	-52.26473236	322.814	RBMC
mtcn	-13.55582523	-52.27135849	423.216	RBMC
mtco	-10.80386353	-55.4562645	307.196	RBMC
mtju	-11.42733002	-58.76931763	363.769	RBMC
mtsf	-11.61927891	-50.66350555	181.822	RBMC
mtsr	-12.54523373	-55.72741318	391.635	RBMC
mtvb	-15.0064249	-59.95155716	219.61	RBMC
naus	-3.022918463	-60.05501556	93.874	RBMC
neia	-25.02023697	-47.92496872	6.025	RBMC
onrj	-22.89569855	-43.2243309	35.612	RBMC
ouri	-22.94917297	-49.89504242	444.834	RBMC
paat	-3.200981617	-52.18130875	162.53	RBMC
pait	-4.287655354	-56.03635788	9.173	RBMC
past	-2.504733086	-54.72197342	130.923	RBMC
pbcg	-7.213675976	-35.90713882	534.089	RBMC
pbjp	-7.136276722	-34.87342453	49.051	RBMC
peaf	-7.764110565	-37.63195419	533.014	RBMC
pepe	-9.38441658	-40.50612259	369.095	RBMC
pisr	-9.030692101	-42.70275879	366.811	RBMC
pitn	-5.102479935	-42.79302979	67.963	RBMC
pitr	-5.102480412	-42.79302979	67.969	RBMC
poal	-30.07404137	-51.11976624	76.719	RBMC
poli	-23.5556469	-46.73031235	730.607	RBMC
pove	-8.709335327	-63.89632034	119.573	RBMC
ppte	-22.11990356	-51.408535	431.013	RBMC
prcv	-24.9627533	-53.46633148	777.267	RBMC
prgu	-25.38399696	-51.48757935	1043.11	RBMC
prma	-23.40968704	-51.93842316	543.303	RBMC
recf	-8.050962448	-34.9515152	20.148	RBMC
riob	-9.965457916	-67.80281067	172.602	RBMC

riod	-22.81784248	-43.30627823	8.605	RBMC
rjcg	-21.76486397	-41.32615662	9.904	RBMC
rnmo	-5.204232216	-37.32546616	23.372	RBMC
rnna	-5.836139202	-35.20770645	45.963	RBMC
rocd	-13.12227535	-60.54391098	451.701	RBMC
rogm	-10.78424168	-65.33060455	157.756	RBMC
roji	-10.86389923	-61.9597168	182.882	RBMC
rosa	-22.52330208	-52.9520874	299.651	RBMC
rsal	-29.78944397	-55.76884079	117.156	RBMC
saga	-0.143853053	-67.05778503	94.891	RBMC
salu	-2.593457937	-44.21247864	18.981	RBMC
savo	-12.93924522	-38.43225479	76.31	RBMC
scaq	-26.39375687	-48.73744202	17.285	RBMC
scch	-27.13756371	-52.59950638	744.183	RBMC
scfl	-27.59937859	-48.51953507	17.009	RBMC
scla	-27.79283333	-50.30426025	940.667	RBMC
seaj	-10.92963123	-37.10427856	1.614	RBMC
sjrp	-20.78551674	-49.35995102	535.876	RBMC
sjsp	-23.20713043	-45.8617363	605.201	RBMC
smar	-29.71892166	-53.7165947	113.097	RBMC
spar	-21.18466377	-50.43978882	410.303	RBMC
spbo	-22.85246658	-48.43230057	803.068	RBMC
spca	-22.81628418	-47.06269455	622.947	RBMC
spja	-21.2410717	-48.28670502	570.171	RBMC
ssa1	-12.97515678	-38.51648331	-2.094	RBMC
togu	-11.74670506	-49.04909897	272.592	RBMC
topl	-10.17105198	-48.33068085	256.536	RBMC
uba1	-23.50017548	-45.1189003	6.156	RBMC
ube1	-18.889534	-48.31697083	791.709	RBMC
uber	-18.889534	-48.31697083	791.777	RBMC
ufpr	-25.44836807	-49.23095322	925.763	RBMC
vico	-20.76149941	-42.8699913	665.942	RBMC
lafl	-9.870464325	-56.10402298	282.509	LISN
lanc	-11.77600002	-77.15000153	60	LISN
laya	-13.1537075	-74.20613098	2803.813	LISN
lbht	-19.86860275	-43.96193314	815.168	LISN
lbo_	4.63778019	-74.08234406	2589.571	LISN
lboa	2.833805799	-60.69459534	69.926	LISN
lbsb	-15.76440525	-47.86919403	1022.989	LISN
lcba	-15.56000042	-56.0699997	247.58	LISN
lchp	-22.70000076	-45.00999832	0	LISN

lcor	-27.46709251	-58.83097076	112.205	LISN
ldou	-22.19599342	-54.93173599	468.562	LISN
lhyo	-12.04241657	-75.32141113	3360.981	LISN
lios	-14.79658985	-39.1723938	44.46	LISN
ljpr	-10.86257553	-61.96207809	182.626	LISN
lleo	-31.80007553	-69.29273987	2517.916	LISN
lman	-3.109719515	-59.9752655	38.993	LISN
lnta	-5.836161137	-35.20770645	46.04	LISN
lpbr	-26.19767952	-52.68943024	815.129	LISN
lpiu	-5.169921398	-80.63934326	53.184	LISN
lpln	-9.36208725	-40.53857803	373.864	LISN
lpmo	-12.58589459	-69.18680573	230.034	LISN
lpts	-19.58204269	-65.75378418	4004.985	LISN
lpuc	-8.383924484	-74.57374573	189.292	LISN
lpvh	-8.837065697	-63.9399147	144.786	LISN
lrbr	-9.957709312	-67.86907196	192.925	LISN
lrib	-10.99965191	-66.08071137	163.698	LISN
lsjk	-23.20757294	-45.85971069	615.337	LISN
lslz	-2.589999914	-44.20999908	0	LISN
lsms	-29.44228935	-53.82195282	492.524	LISN
lsta	-29.71264648	-53.7173233	107.313	LISN
lstf	-32.95934296	-60.6284256	66.608	LISN
lstm	-2.428311348	-54.73134995	11.026	LISN
ltca	-26.81395912	-65.25567627	482.737	LISN
ltfe	-3.348725557	-64.72094727	64.666	LISN
lvlg	-35.0326004	-63.01364136	148.697	LISN
FORT	-3.744553804	-38.5776329	22.294	CIGAL
GALH	-22.12150574	-51.41606903	425.245	CIGAL
INCO	-22.3185482	-46.32811356	884.923	CIGAL
MAC2	-22.3768158	-41.79138565	84.115	CIGAL
MAN2	-3.091880083	-60.01726151	28.883	CIGAL
MANA	-3.119825363	-60.00716782	72.773	CIGAL
MORU	-22.1276741	-51.41329956	454.522	CIGAL
PALM	-10.19964886	-48.31129837	272.735	CIGAL
PRU1	-22.12004471	-51.40867233	433.117	CIGAL
PRU2	-22.12203789	-51.40707779	441.816	CIGAL
PRU3	-22.11908531	-51.40603638	418.596	CIGAL
SJCE	-23.20752716	-45.85974503	615.218	CIGAL
SJCU	-23.21058846	-45.95659256	608.05	CIGAL
afae	-21.98956108	-47.3333931	599.481	ICEA
afaw	-21.98992539	-47.33418274	599.889	ICEA

baaf	-22.88010979	-43.3833046	33.955	ICEA
bacg	-20.4662056	-54.66188049	565.66	ICEA
basc	-22.93831635	-43.71730804	3.324	ICEA
eear	-22.78900719	-45.22447586	549.178	ICEA
gevt	-22.90944862	-43.16781616	13.528	ICEA
gltw	-22.80986023	-43.25036621	47.715	ICEA
icea	-23.20812416	-45.86962891	602.303	ICEA
pcot	-22.46533012	-43.29206848	1756.745	ICEA
bgl1	-22.79899292	-43.25156219	1.864	HNYWL
bgl2	-22.79080598	-43.21432458	4.544	HNYWL
bgl3	-22.82952315	-43.23642254	0.652	HNYWL
bat1	-4.509485245	-65.52911377	59.759	SIPEG
bepa	-1.460806966	-48.44140625	-17.814	SIPEG
caam	-4.870801926	-66.89636231	98.951	SIPEG
chrn	-3.119836092	-60.00716782	72.815	SIPEG
coam	-4.097809792	-63.14507675	37.947	SIPEG
embp	-2.890505552	-59.96981049	100.301	SIPEG
inpa	-3.095891476	-59.98971558	85.672	SIPEG
itbr	-20.50904465	-29.30890656	3.671	SIPEG
jamg	-15.36270523	-43.76685333	475.372	SIPEG
pcsp	-22.7030468	-47.62361908	561.904	SIPEG
ptmg	-18.53201485	-46.43499374	1067.455	SIPEG